Graphene-based Artificial Nacre Nanocomposites

Journal:	*Chemical Society Reviews*
Manuscript ID	CS-SYN-03-2015-000258.R3
Article Type:	Tutorial Review
Date Submitted by the Author:	15-Feb-2016
Complete List of Authors:	Cheng, Qunfeng; Beihang University, Zhang, Yuanyuan; Beihang University, Gong, Shanshan; Beihang University, Zhang, Qi; Beihang University, Ming, Peng; Beihang University, Wan, Sijie; Beihang University, Peng, Jingsong; BeiHang University Jiang, Lei; Beihang University,

Graphene-based Artificial Nacre Nanocomposites

Yuanyuan Zhang[†], Shanshan Gong[†], Qi Zhang, Peng Ming, Sijie Wan, Jingsong Peng, Lei Jiang, and Qunfeng Cheng*
Key Laboratory of Bio-Inspired Smart Interfacial Science and Technology of Ministry of Education, School of Chemistry and Environment, BeiHang University, Beijing 100191, P. R. China

E-mail: cheng@buaa.edu.cn

These two authors contributed equally to this work.

Abstract

With its extraordinary properties as the strongest and stiffest material ever measured and the best-known electrical conductor, graphene could have promising applications in many fields, especially in the area of nanocomposites. However, processing graphene-based nanocomposites is very difficult. So far, graphene-based nanocomposites exhibit rather poor properties. Nacre, the gold standard for biomimicry, provides an excellent example and guidelines for assembling two-dimensional nanosheets into high performance nanocomposites. The inspiration from nacre overcomes the bottleneck of traditional approaches for constructing nanocomposites, such as poor dispersion, low loading, and weak interface interactions. This tutorial review summarizes recent research on graphene-based artificial nacre nanocomposites and focuses on the design of interface interactions and synergistic effects for constructing high performance nanocomposites. This tutorial review also focuses on a perspective of the dynamic area of graphene-based nanocomposites, commenting on whether the concept is viable and practical, on what has been achieved to date, and most importantly, what is likely to be achieved in the future.

Key learning points

(1) The nacre-inspiration assembly approach

(2) The strategies for interface interaction design

(3) Synergistic effects from interface interactions

(4) Synergistic effects from building blocks

(5) Guidelines for designing graphene-based artificial nacre nanocomposites

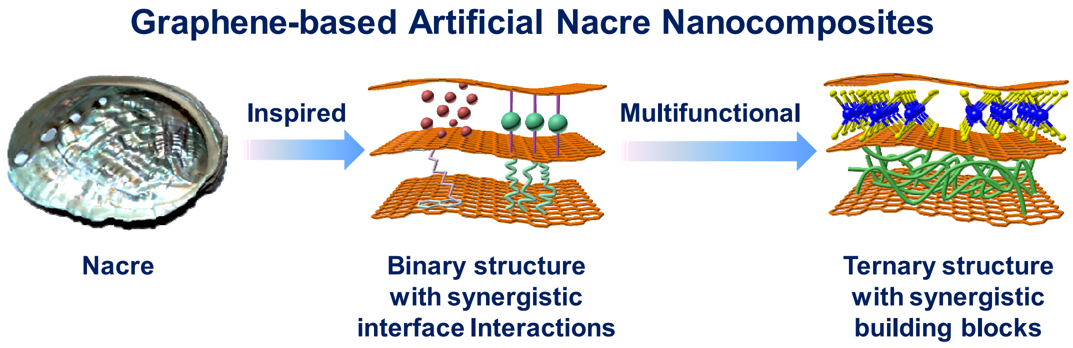

1. Introduction

With its extraordinary properties as the strongest and stiffest material ever measured and the best-known electrical conductor, graphene[1] could have promising applications in many fields, especially in the area of composites.[2] However, processing graphene-based composites is very difficult. So far, graphene-based nanocomposites fabricated through traditional approaches exhibit rather poor properties, for example, the tensile strength and toughness of graphene-based composites show a little bit improvement compared with the pure polymer matrix. The main bottlenecks of traditional approaches are poor dispersion and low loading of graphene in polymer matrix, and weak interface interactions between graphene and polymer matrix. It is a great challenge to assemble these micro-scale nanosheets into macro-sized nanocomposites for practical applications, for example, in aerospace, as flexible supercapacitor electrodes, and in artificial muscle and tissue engineering.

Since 2011 there have been several main reviews on graphene-based nanocomposites. Huang *et al.*[3] reviewed the various methods for preparing graphene-based nanocomposites and applications for these nanocomposites. Young *et al.*[4] reviewed different techniques for preparing graphene and graphene oxide (GO) and their structure and mechanical properties. Young *et al.*[4] also described bulk nanocomposites based on graphene and GO, and they concluded that good reinforcement is only at relatively low levels of graphene loading. Due to the difficulties in obtaining good dispersion, challenges still remain in achieving high performance for high volume fractions of the reinforcement. Wu *et al.*[5] focused on the self-assembly strategies of chemically modified graphene and nanomaterials and highlighted the representative applications. Yang *et al.*[6] critically evaluated the layer-by-layer assembly technique and made comparisons with other assembly approaches for fabricating graphene-based nanocomposites. They also discussed the applications of graphene-based nanocomposites. Sun *et al.*[7] mainly described the preparation, structure, properties, and applications of nanocomposites based on carbon nanotubes and graphene, emphasizing the differences between them. Recently, Hu *et al.*[8] reviewed the most significant results of polymer-graphene nanocomposites, and discussed some fundamental properties and the processing approaches of such nanocomposites. Although descriptions of different methods for preparing graphene-based nanocomposites have been provided in the above mentioned reviews, we are aiming here for something different and more critical. Our notion is not simply to write a review, but to provide some inspiration to the community and a clear vision for the future.

Where might one seek inspiration for making something new and original? None of the reviews published so far highlighted the possibility of using a bioinspired approach for making these materials.

Nacre, the “gold standard” for biomimicry with both high strength and toughness due to billions of years of evolution, has been the source of inspiration for designing many synthetic hybrid materials and nanocomposites.[9-13] The unique structure of nacre shows: (i) a “brick and mortar” layered architecture alternatively packed with 95 vol.% of two-dimensional (2D) aragonite calcium carbonate platelets, and 5 vol.% of one-dimensional (1D) nanofibrillar chitin and protein, and (ii) different interface interactions between inorganic platelets and organic protein. This is achieved through a precise architecture resembling that of a brick wall and the clever design of the interface. The prospect of nature-inspired design to develop new synthetic nanocomposites is very enticing. Advances in diverse fields such as aerospace, building design, transportation, energy, and tissue engineering require the development of new, high performance structural materials. In many respects, graphene-based nanocomposites are ideal candidates. Compared with other approaches for constructing graphene-based nanocomposites, this bioinspired concept results in good dispersion, high loading, and excellent interface interaction design. The resultant graphene-based nacre-like nanocomposites demonstrate significant enhancement in mechanical and electrical properties. The creation of nacre-inspired materials with intricate, hierarchical architectures is a challenge that requires both the design of optimum microstructures and the development of fabrication procedures to implement these designs.

In this tutorial review, we summarize recent research on graphene-based artificial nacre nanocomposites and discuss novel assembly strategies of graphene-based artificial nacre nanocomposites with different interface design. We highlight the fundamental properties of graphene-based artificial nacre nanocomposites, such as tensile strength, toughness, and electrical conductivities. We hope to convince the wider scientific community that by mimicking natural structural architectures and identifying/incorporating the salient strengthening/toughening mechanisms at multiple length-scales, a new suite of unique lightweight and structural nanocomposites can be developed. Finally, we offer a perspective on how to construct integrated graphene-based artificial nacre nanocomposites through the synergistic effect from interface interactions and building blocks, providing some inspiration to the community and a clear vision for the future of integrated graphene-based artificial nacre nanocomposites.

1.1 Layered structure and interface design of natural nacre

Nacre is a brick-and-mortar structure showing an ordered layered structure with inorganic $CaCO_3$ mineral platelets (aragonite) and organic layers, in which the hexagonal $CaCO_3$ mineral platelets are 5~8 μm in diameter and ~0.5 μm in thickness, and the organic layers, which have a thickness of ~10-50 nm, contain acidic proteins and a chitin network,[14] as shown in Figure 1A. Recent investigation demonstrated that the $CaCO_3$ mineral platelets are comprised of millions of nanograins (~30 nm), as shown in Figure 1B. Several typical types of interface between alternatively ordered $CaCO_3$ platelets have been categorized as follows[9]: (i) mineral bridges between $CaCO_3$ platelets; (ii) nano-asperities for shearing resistance; (iii) organic glue; and (iv) tablet interlocking. The hallmark property of nacre is toughness, which is almost three orders of magnitude higher than that of monolithic calcium carbonate.[9] As shown in Figure 1B, nacre's toughness mostly depends on its abundant interface. The cracks in nacre can be deflected around the orderly layered structure. Such deflection dissipates more energy than a straight crack, as shown in Figure 1C. Munch *et al.*[15] demonstrated the high performance bioinspired alumina (Al_2O_3)/polymethyl methacrylate (PMMA) ceramic materials, which shows higher bending strength than the natural nacre, as shown in Figure 1D. Meanwhile, the fracture toughness is also higher than that of natural nacre, as shown in Figure 1E. This kind of bioinspired Al_2O_3/PMMA ceramic materials provides a new mechanism to achieve high mechanical properties over that of traditional mixture mechanism through constructing the orderly hierarchical structure and abundant interface interactions between inorganic and organic constituents.

1.2 Extraordinary properties of graphene and graphene oxide

Graphene, a novel 2D carbon nanomaterial, possesses extraordinary physical properties due to its pure sp^2 hybridization network.[1] For example, graphene's tensile strength reaches ~130 GPa, its strain is as high as 25%, and its electrical conductivity is up to 6 × 10^3 S/cm. These outstanding properties allow graphene to have numerous promising applications in the fields of aerospace, as flexible supercapacitor electrodes, and in artificial muscle and tissue engineering.[1] Pristine graphene can be obtained by the top-down method of mechanical exfoliation and the bottom-up method of chemical vapor deposition.[1] However, these methods are time consuming, and have limited ability to scale up to create graphene nanosheets. The precursor of graphene, GO, is usually obtained by Hummers' method through chemically functionalizing mineral graphite flakes, which is an efficient and versatile option. Meanwhile, the resulting single atomic layer GO possesses a high density of epoxide and hydroxyl groups on both its surfaces and carboxyl groups around its edges. These functional groups allow GO itself to be used in nanocomposites, especially for nacre-like layered materials, through interface interactions design.

2. Interface interactions for graphene-based artificial nacre nanocomposites

GO is an ideal candidate to be a 2D building block for constructing artificial nacre nanocomposites through interface interactions design due to abundant functional groups on the surface of GO. The interface strength of resultant graphene-based artificial nacre nanocomposites is dramatically enhanced, resulting in high efficiency of load transfer and improved mechanical properties. Recently, a series of papers have reported different kinds of interface interactions, which can be categorized into two classes: (i) non-covalent bonding and (ii) covalent bonding, as shown in Figure 2. Non-covalent bonding, mainly containing hydrogen bonding, ionic bonding, and π-π interaction, demonstrates relatively weak interaction compared with covalent bonding through chemical reactions. In many natural materials, there is more than one kind of interface interactions. Thus, the combination of interface interactions can be also designed in graphene-based artificial nacre nanocomposites, as shown in Figure 2. The corresponding mechanical properties of graphene-based artificial nacre nanocomposites can also be tuned through designing different combinations of interface interactions. In the following sections of this review, different interface interactions and synergistic interactions are discussed in detail. In this tutorial review, toughness is defined as the amount of energy the material absorbs before it fails under tensile stretching,[14] expressed as the following equation:

$$U = \int_0^{\varepsilon_f} \sigma d\varepsilon$$

where U is the energy per volume absorbed, $\sigma$is the stress, ε is the strain, and ε_f is the failure strain.

2.1 Hydrogen bonding

Weak hydrogen bonding exists in many natural materials. For example, bone exhibits excellent fracture toughness due to sacrificial hydrogen bonding between mineralized collagen fibrils.[14] High performance GO-based layered materials were first demonstrated by Dikin *et al.*[16] through a vacuum-assisted assembly GO water solution in 2007, as shown in Figure 3A. The cross-section surface morphology demonstrates the GO nanosheets' orderly structure, as shown in Figure 3B. The high strength of 133 MPa and Young's modulus of 32 GPa are attributed to rich hydrogen bonding between the adjacent GO nanosheets and residual water molecules in the fabrication process. Furthermore, Medhekar *et al.*[17] further investigated the effect of hydrogen bonding networks on the mechanical properties of GO paper through molecular dynamic simulations with reactive force fields. Figure 3C schematically illustrates various configurations of hydrogen bonding in hydrated GO paper. Hydrogen bonding can be formed not only between the functional groups on the GO nanosheet, but also between GO and water molecules. The results of molecular dynamics simulations show that the mechanical properties of GO paper are essentially controlled by hydrogen bonding networks involving both functional groups on GO nanosheets, as well as water molecules in the interlayer cavities. Medhekar *et al.*[17] suggested the possibility of tuning the mechanical properties of GO paper through altering the number of hydrogen bonding networks between GO nanosheets and interlayer water molecules.

Compared with water molecules, an organic polymer with hydroxyl groups or oxygen groups is much better for constructing hydrogen bonding in GO-based artificial nacre nanocomposites (for example, poly[vinyl alcohol] [PVA] and poly[methyl methacrylate] [PMMA]). Putz *et al.*[18] demonstrated GO-based artificial nacre nanocomposites with PVA and PMMA (designated as GO-PVA, and GO-PMMA). Hydrogen bonding networks are formed between pendant hydroxyl groups of PVA chains and oxygen-containing groups on GO nanosheets, as shown in Figure 3D. Compared with water molecules, the hydroxyl groups of PVA can also act as both hydrogen bonding acceptors and donors. Furthermore, the covalent C-C bonds in the PVA chain further link the hydrogen bonding into a multiconnected bridge, resulting in much stronger interface interactions. The storage modulus of GO-PVA nanocomposites exceeds a simple rule-of-mixture calculation with GO and PVA compounds. For example, GO-PVA nanocomposites with 77.4 wt.% GO show a storage modulus of 36.3 GPa, which is two times higher than that of the value calculated from rule-of-mixture. Different from

PVA, the moduli of GO-PMMA nanocomposites were only minimally affected by the PMMA filler content. This is because PMMA can act only as a hydrogen bonding acceptor through the ester functional groups on the side chain, as shown in Figure 3D. Furthermore, the hydrophobicity and steric hindrance of the methyl groups of the methacrylate side chains would further limit the weak interactions between GO and PMMA, leading to the lower moduli of GO-PMMA nanocomposites, and closely adhering to the rule-of-mixture calculation.

Li *et al.*[19] demonstrated higher mechanical properties of GO-PVA nanocomposites with hydrogen bonding. The reason for this may be the large size of GO nanosheets used. After being chemically reduced, the reduced GO-PVA (rGO-PVA) nanocomposites show dramatic improvement in tensile strength with 188.9 MPa. Although the hydrogen bonding networks may be destroyed with chemical reduction of GO nanosheets, due to the removing of oxygen-containing groups on the GO nanosheets, the interlayer spacing will dramatically decrease, resulting in the much stronger interactions of π-π stacking between reduced GO nanosheets. This may be the underlying reason why high mechanical properties can be obtained after chemically reducing GO-PVA nanocomposites.

Compton *et al.*[20] further applied a joint experimental-theoretical and computational simulation to reveal a delicate relationship between the stiffness of GO papers and water content. The cooperativity of the hydrogen bonding network can be further enhanced by a PVA chain in the GO-PVA nanocomposites, resulting in increased stiffness of the GO-PVA nanocomposites. Figure 3E shows the model snapshot highlighting the hydrogen bonding network in the GO-PVA nanocomposites with 5.5 wt.% PVA and 15 wt.% water. The results reveal that the cooperative interactions of hydrogen bonding networks in the intersheet gallery enhance the stiffness of the GO-PVA nanocomposites in a similar fashion found in natural biocomposites, such as spider silk and collagen. These findings can act as guidance for tuning mechanical properties of other layered composites with interface interactions of hydrogen bonding networks in the future.

2.2 Ionic bonding

A small amount of metal ion in the protein structure of some biomaterials leads to extraordinary mechanical properties. For example, metals such as zinc and cooper play a role in mechanical hardening of the jaws of the marine polychaete worm Neries.[21] Other metals, including manganese, calcium, titanium, aluminum, and iron, can also enhance the mechanical properties of biomaterials, especially the stiffness and hardness.[21] Inspired by this correlation between metal elements and the mechanical properties of biomaterials, Park *et al.*[22] introduced the metal elements of calcium and magnesium (less than 1 wt.%) in the gallery of GO nanosheets through formation of ionic bonding with GO nanosheets to enhance the mechanical properties of GO paper. The characterizations of Fourier transform infrared spectroscopy (FTIR), X-ray photoelectron spectroscopy (XPS), and Raman spectra demonstrated that carboxylic acid coordinates to a divalent metal ion, resulting in the cross-linking GO nanosheets. The reactive epoxy groups on the GO surface have led to ring-opening of the epoxide groups at exposure to Lewis acidic divalent metal ions such as Ca^{2+}, Mg^{2+}, *et al*. The analytical results indicated that the alkaline earth metal ions interact with GO nanosheets by two different bonding modes. The extent of interaction depended on the nature of the metal ions themselves. As shown in Figure 4A, two modes of interactions between alkaline earth metal ions and GO nanosheets were suggested: (i) bridging the edges of the GO nanosheets through carboxylate chelates to the metal, and (ii) intercalating between the basal planes through either weak alkoxide or dative bonds from carbonyl and hydroxyl groups. They concluded that the first kind of ionic bonding mode is stronger that the second. The metal ions entered the gallery of GO nanosheets of GO-based nanocomposites, which increased the *d*-spacing and the cross-sectional area of the tensile sample, resulting in an overall reduction of tensile strength. At this point, the size of the intercalated metal ions greatly contributes to the mechanical properties of GO-metal ion nanocomposites. For example, the GO-Mg^{2+} nanocomposites show high mechanical properties with a tensile strength of 87.9 MPa and a Young's modulus of 24.6 GPa. These properties are higher than those of GO-Ca^{2+} nanocomposites, which have a tensile strength of 75.4 MPa and Young's modulus of 21.5 GPa. This is because the ionic radius of Mg^{2+} is 0.78 Å, which is lower than the Ca^{2+} radius of 1.06 Å.

The other feature of the ionic bonding is that the bonds between alkaline earth metal ions and carboxylate/hydroxyl groups can be reversibly exchanged. The concept of "mechanically annealed" means that the edge-bound metal ions that adopt more favourable chemical interactions with the oxygen functionalities of GO nanosheets would be obtained through repeated cyclic loading of GO-metal ion nanocomposites with small amount of force at a slow rate. The tensile strength and Young's modulus of rinsed GO-Ca^{2+} nanocomposites are significantly improved to 125.8 MPa and 28.1 GPa from 75.4 MPa and 21.5 GPa for the as-prepared GO-Ca^{2+} nanocomposites.

Recently, Yeh *et al.*[23] discovered that the stability of GO papers in water can be attributed to the cross-linking of multivalent metal cations during the purification process, such as Al^{3+}. In particular, the porous anodized aluminium oxide (AAO) filter discs used in filtration processing can corrode, releasing a significant amount of Al^{3+} that cross-links the GO nanosheets and significantly strengths the GO papers, as shown in Figure 4B. GO-Al^{3+} nanocomposites with a tensile strength of 100.5 MPa and a Young's modulus of 26.2 GPa are much stronger and stiffer than pure GO paper with a tensile strength of 86.9 MPa and a Young's modulus of 7.6 GPa. Park *et al.*[22] showed around 10% improvement in stiffness of GO papers after cross-linking with divalent metal ions. However, Yeh *et al.*[23] demonstrated 340% enhancement in stiffness with Al^{3+} cross-linking. This difference is because the GO papers used by Park *et al.*[22] were also obtained with an AAO filter. Therefore, the as-control GO papers were probably already cross-linked with ionic bondings of Al^{3+}, resulting in only a modest stiffness difference between as-control and cross-linked GO papers. On the other hand, this interlayer of Al^{3+} ions can be removed from GO papers by ionic exchange with hydrochloric acid or other multivalent cations, which demonstrates the potential of swollen GO papers for the templated synthesis of new 2D nanomaterials with lamellar structures.

In fact, other divalent ions have also been used to cross-link the GO nanosheets. For example, Jiang *et al.*[24] realized a gel-like three dimensional (3D) reduced GO structure via divalent ions (Ca^{2+}, Ni^{2+}, or Co^{2+}) connecting rGO nanosheets. As shown in Figure 4C, the rGO nanosheets' skeleton is interconnected and supported by the ionic bonding and hydrogen bonding between the divalent metal ions, water molecules, and the oxygen-containing groups on the rGO surface. This study provides a facile and practical route to prepare the 3D rGO architecture through ionic bonding.

Different from the aforementioned approaches for constructing the GO-based nanocomposites with ionic bonding, Lam *et al.*[25] reported an one-pot post-processing method to fabricate robust and conductive GO-based nanocomposites through impregnating a small amount of zinc by atomic layer deposition (ALD). The self-limited growth nature of ALD allowed the zinc metal to infiltrate GO paper using H_2O as an oxygen source. H_2O vapor absorbed on the GO paper surface forms a hydroxyl group, which reacts with the zinc metal. The proposed reaction mechanism is that the zinc impregnated in the interlayers of the GO paper and bridged GO nanosheets through ionic bonding with the oxygenated groups on GO surface, as shown in Figure 4D. The mechanical and electrical properties of the GO-Zinc nanocomposites were dramatically improved. For example, the tensile strength and stiffness of GO-Zinc nanocomposites reach ~142.2 MPa, and ~35.4 GPa, corresponding to ~27% and ~20% than that of pure GO papers with a tensile strength of ~112 MPa and stiffness of ~29.5 GPa, respectively. The electrical conductivity of GO-Zinc nanocomposites reaches ~0.01 S/cm, which is three orders of magnitude higher than that of pure GO papers. This may be due to the thin conductive ZnO layer deposited on the GO surface and the impregnated Zn atoms cross-linking GO nanosheets. The other reason was attributed to the ionic bonding between zinc ions with GO nanosheets. Meanwhile, this GO-Zinc nanocomposites can be used to selectively separate diverse organic vapors with unimpededly permeating water, which may be used for separation and purification technology.

2.3 π-π interaction

With similar principles, conjugated molecules with pyrene derivative have been used as the cross-linker to improve the solubility of a single graphene nanosheet and the interface strength between adjacent graphene nanosheets. Xu *et al.*[26] reported rGO-based nanocomposites with π-π interaction using a water soluble pyrene derivative (1-pyrenebutyrate) (PB). The flexible assembled rGO-based nanocomposites (rGO-PB) are shown in Figure 5A, and the cross-section image indicates the nanocomposites' well-packed layered structure. After π-π interaction with PB, the resultant rGO-PB nanocomposites show high mechanical and electrical properties. For example, the tensile strength and modulus of rGO-PB nanocomposites reach 8.4 MPa and 4.2 GPa, respectively, comparable to those of flexible graphite foils composed of stacked platelets of expanded graphite. The electrical conductivity is about 2 S/cm, almost seven orders of magnitude higher than the pure GO paper.

Liu *et al.*[27] demonstrated great improvement in plane-to-plane tunnelling conductivity of stacked graphene layers through π-π interaction between pyrene derivative and graphene nanosheets. Several other molecules with similar pyrene structures, such as 1-pyrenebutyric acid N-hydroxysuccinimide ester, 1-Pyrenebutyric acid, 1-Pyrenebutanol, 1-Pyreneacetic acid, 1-Pyrenecarboxylic acid, and Pyrene-1-boronic acid had also been attempted by Liu *et al*.[27] However, these molecules are prone to aggregation, producing deleterious effects on conductivity.

Teng *et al.*[28] synthesized pyrene molecules with a functional segmented poly(glycidyl methacrylate) (Py-PGMA) through an atom transfer radical polymerization polymer chain. The adjacent graphene nanosheets were strongly adhered by Py-PGMA through π-π interactions, as shown in Figure 5B. They concluded that epoxide groups on the Py-PGMA could react with epoxy resin to form a covalent cross-linking structure, resulting in high thermal conductivity of the resultant nanocomposites. Zhang *et al.*[29] functionalized polyethylene glycol (PEG) with the introduction of the pyrene groups. Functionalized PEG (FPEG) was used to improve the interface interactions of adjacent graphene nanosheets. As shown in Figure 5C, the adjacent graphene nanosheets were bridged by the FPEG through π-π interaction. During loading, the FPEG chains were stretched along the sliding direction, absorbing a large amount of energy. With further loading, the π-π interaction between FPEG and graphene nanosheets would be broken, resulting in much more energy dissipation. Thus, the tensile strength of resultant nanocomposites (rGO-FPEG) was greatly improved to 45 MPa from 15 MPa for pure rGO film. Meanwhile, the effect of the molecule length of PEG on the mechanical properties was also investigated. The results revealed that long molecular FPEG can link adjacent graphene nanosheets into a network; however, the FPEG with a short molecular chain may adsorb on the same graphene nanosheet. Thus the long molecular FPEG is better for improving the mechanical properties of resultant nanocomposites through π-π interactions.

2.4 Covalent bonding

Compared with non-covalent bonding, covalent bonding shows greater robustness, and many molecules and polymers have been utilized to construct covalent bonding between adjacent graphene nanosheets. Gao *et al.*[30] applied the small molecule of glutaraldehyde (GA) to react with the hydroxyl groups on the surface of the GO nanosheets *via* intermolecular acetalization. The tensile strength and Young's modulus of GO-GA nanocomposites increased from 63.6 MPa and 10.5 GPa to 101 MPa and 30.4 GPa, respectively. The covalent cross-linking with a short molecule between GO nanosheets may not be good enough to improve the interface strength due to the short cross-linking chain and low covalent bonding density between adjacent GO nanosheets. Thus, much higher covalent cross-linking density would be better. For example, An *et al.*[31] demonstrated graphene-based nanocomposites with high strength and stiffness through forming borate oligo-orthoesters between adjacent GO nanosheets, as shown in Figure 6A. The covalent borate orthoester bonds were formed through hydroxyl moieties on the surface of GO with sodium borate. These covalent bonding networks result in great improvement of mechanical properties. For example, the tensile strength and stiffness are enhanced from 130 MPa and 30 GPa to 160 MPa and 110 GPa, as shown in Figure 6C. Further thermal annealing resulted in the formation of more covalent bonding between sodium borate and adjacent GO nanosheets through dehydration. And the mechanical properties of GO-Borate nanocomposites were further improved to 185 MPa for tensile strength and 127 GPa for modulus.

On the other hand, a high tensile strength and Young's modulus can also be achieved through constructing a three dimensional network of covalent bonding between adjacent GO nanosheets. For example, Tian *et al.*[32] constructed a covalent bonding network between polydopamine (PDA) coated on GO nanosheets and polyetherimide (PEI), as shown in Figure 6B. The catechol groups in PDA would be oxidized into quinone under a weak alkaline environment with a pH of 8.5, and the quione covalently cross-links with the amine groups on the PEI. When the PEI loading reaches about 14.7 wt.%, the mechanical properties achieve the maximum value with a tensile strength of 179.0 MPa and Young's modulus of 84.8 GPa. With further orientation of GO nanosheets by vacuum assisted filtration, the strength and Young's modulus of PGO-PEI nanocomposites can reach 209.9 MPa and 103.4 GPa. These values correspond to an 80% and 238% improvement compared with the pure GO film, which has a tensile strength of 116.1 MPa and 30.6 GPa. However, the elongation decreases to ~0.24% from ~0.66%, resulting in low toughness, because the enhanced interlayer interaction between GO nanosheets prevents adjacent GO nanosheets from slipping.

Recently, Jia *et al.*[33] used dicarboxylic acid, dios, or polyols to covalently cross-link GO nanosheets through esterification reactions, as shown in Figure 6D. The intersheet spacing, and elastic moduli of resultant nanocomposites can be adjusted through altering the chain length, functional groups, and substituents of cross-linkers. This kind of artificial nacre nanocomposite focuses on the precise separation of ions and molecules, which makes it very difficult to compare them with other graphene-based artificial nacre nanocomposites.

Based on the aforementioned works, high toughness would be achieved when introducing a long chain of cross-linker between adjacent GO nanosheets through covalent bonding. Thus, Cheng *et al.*[34] applied a long chain linear molecule, 10, 12-pentacosadiyn-1-ol (PCDO), to covalently cross-link GO nanosheets, as shown in Figure 7A. Firstly, the PCDO linear molecules were grafted with GO nanosheets through esterification reaction between the alcohol groups at one end of the PCDO and the carboxylic acids on the surface of the GO nanosheets. Then, the PCDO molecules were further cross-linked with each other through 1,4-addition polymerization of their diacetylenic units under UV irradiation. Then, the network of cross-linker PCDO was formed between adjacent GO nanosheets, not only improving the load transfer but also proving the electron-transfer pathway among the Z direction of GO nanosheets. Finally, the residual groups on the GO nanosheets were removed by hydroiodic acid (HI). The tensile stress-strain curves are shown in Figure 7B. With cross-linking of PCDO networks, the tensile strength and toughness of graphene-based artificial nacre nanocomposites reach 129.6 MPa and 3.9 MJ/m^3, respectively, which corresponds to 36% and 117% improvement for pure GO film.

The origin of improvement in the mechanical properties of graphene-based artificial nacre nanocomposites can be revealed by unique fracture morphology, as shown in Figure 7C. GO nanosheets were pulled out in the fracture process and the edges of GO nanosheets were dramatically curved, indicating the strong covalent bonding between PCDO molecules and GO nanosheets. After chemical reduction, identical fracture morphology was clearly observed and the edges of graphene nanosheets were even more strongly curved. The proposed fracture process of graphene-based artificial nacre nanocomposites is shown in Figure 7D. The network of PCDO molecules cross-linked with graphene nanosheets is firstly coiled between adjacent graphene nanosheets. During loading, the weak hydrogen bonding in graphene-based artificial nacre nanocomposites is firstly ruptured and the coiled PCDO network is stretched along the sliding direction of graphene nanosheets, dissipating a large amount of energy. When the loading is further increased, the covalent bonding between PCDO and adjacent graphene nanosheets, as well as the ene-yne backbones of network of PCDO molecules, are simultaneously broken, leading to curving of the graphene nanosheets.

Different from covalent bonding between linear molecules and GO nanosheets, the linear polymer is expected to dramatically enhance mechanical properties due to the long molecule chain. For example, Park *et al.*[35] demonstrated covalent bonding between polyallylamine (PAA) and GO nanosheets. Many reactive amine groups on the long alky chain of PAA were supposed to be reacted with the groups of epoxide and carboxylic acid on the surface of GO nanosheets. The tensile strength and Young's modulus of GO-PAA nanocomposites increased to 91.9 MPa and 11.3 GPa from 81.9 MPa and 5.8 GPa for pure GO paper, respectively.

3. Synergistic effect

In fact, a synergistic effect has always existed in natural materials.[14] Nacre, which contains abundant interfacial interactions, including weak and strong interactions, and different surface morphology of $CaCO_3$ platelets,[9] is a good example. These characterizations of natural nacre form all kinds of synergistic effects, which may come from the interface interactions and building blocks of $CaCO_3$ platelets. For graphene-based artificial nacre nanocomposites, these inspirations have been demonstrated through constructing different synergistic effects from interface interactions and building blocks, which are reviewed in detail as follows.

3.1 Synergistic effect from interface interactions

As shown in Figure 2, we categorize six kinds of synergistic interface interactions in this tutorial review. Until now, three kinds of synergistic interface interactions have been successfully demonstrated in graphene-based artificial nacre nanocomposites, which are reviewed in the following sections.

3.1.1 Combination of hydrogen bonding, polar, and hydrophobic interactions

Silk materials are one of the strongest elastomeric biomaterials due to silk's hierarchical multidomain morphology and advanced secondary structure with antiparallel β-sheet nanocrystals. Hu *et al.*[36, 37] demonstrated high mechanical performance graphene-based nanocomposites with a matrix of silk fibroin through heterogeneous interface interactions. For example, the ultrathin nanocomposite membrane of GO nanosheets and silk fibroin (GO-SL), assembled in a layer-by-layer process,[36] shows an ultimate tensile strength of 300 MPa, toughness of 2.2 MJ/m^3, and tensile modulus of 145 GPa.

These outstanding mechanical properties are attributed to the dense network of weak interactions between the silk fibroin domains and GO nanosheets, including hydrogen bonding, and polar-polar and hydrophobic-hydrophobic interactions. Based on the above study, Hu *et al.*[37] further demonstrated integrated rGO-SL nanocomposites with electrical conductivity by a spatially localized electrochemical reduction. The ultimate tensile strength reaches 300 MPa and the toughness is as high as 2.8 MJ/m^3, which may be also caused by additional cross-linking of silk fibroin backbones besides the synergistic interactions of hydrogen bonding, polar, and hydrophobic interactions.

3.1.2 Combination of π-π interaction and hydrogen bonding

Based on the hydrogel casting technique for fabricating the 2D graphene-based film developed by Shi *et al.*,[38] Zhang *et al.*[39] demonstrated high performance graphene-based artificial nacre nanocomposites through a synergistic effect from π-π interaction and hydrogen bonding. The phenylboronic acid moieties were introduced into side chains of poly(acrylic acid) (PAA) as poly(acrylic acid-co-(4-acrylamidophenyl) boronic acid) (PAPB), resulting in formation of π-π interaction besides the hydrogen bonding between adjacent GO nanosheets. The synergistic interactions from π-π interactions and hydrogen bonding interlock intimately with GO nanosheets into rGO-PAPB nanocomposites, not only increasing the strain at break, but also providing more interfacial areas available for stress transfer between GO layers. Thus, the high tensile strength and toughness of rGO-PAPB nanocomposites reached 382 MPa and 7.50 MJ/m^3, respectively, as well as a high electrical conductivity of 337 S/cm.

3.1.3 Combination of covalent and hydrogen bonding

Cui *et al.*[40] applied dopamine (DA), a mimic of the specialized mussel adhesive protein, as an organic matrix to construct graphene-based artificial nacre nanocomposites. DA contains both the functional catechol and amine groups, which not only react with GO nanosheets but also self-polymerize into long chain polymers of poly(dopamine) (PDA). The strong covalent bonding between GO and PDA results in high tensile strength, and the abundant hydrogen bonding network between PDA and adjacent GO nanosheets leads to high tough rGO-PDA artificial nacre nanocomposites. Compared with artificial nacre of rGO-PCDO with only covalent bonding,[34] this kind of synergistic effect of the combination of covalent and hydrogen bonding results in integrated mechanical properties. The tensile strength of rGO-PDA artificial nacre nanocomposites reaches

204.9 MPa, higher than that of rGO-PCDO artificial nacre nanocomposites with 129.6 MPa, and the toughness is as high as 4.0 MJ/m^3, which is a little bit higher than that of the rGO-PCDO artificial nacre nanocomposites with 3.91 MJ/m^3.[34]

This study inspired us to choose biomolecules for constructing integrated graphene-based artificial nacre nanocomposites through the synergistic interactions of covalent and hydrogen bonding. Thus, based on this inspiration, Wan *et al.*[41] demonstrated integration of highly strong and tough GO-based artificial nacre with chitosan (CS) through synergistic interactions of covalent and hydrogen bonding. CS has many functional groups of hydroxyl and amine, and is introduced as a “soft” component for constructing artificial nacre through vacuum-assisted filtration. The proposed mechanism is shown in Figure 8A. When the CS content is low, the flow force spreads the CS molecular chains on the surface of GO, resulting in the formation of intermolecular hydrogen bonding. Then the buried reaction sites (amine) distributed on the CS are exposed and react with carboxyl groups on the surface of GO nanosheets. By contrast, for high CS content, “electrosteric stabilization” leads to strong repulsion during the assembly process. Thus the distribution of the coiled CS with intramolecular hydrogen bonding on the GO nanosheets is very difficult to achieve. A chemical reaction between GO nanosheets and CS cannot occur, and therefore the primary interface interaction is hydrogen bonding.

Compared with the pure GO and CS film, the tensile strength and toughness of GO-CS artificial nacre nanocomposites are dramatically improved to 526.7 MPa, and 17.7 MJ/m^3, respectively, as shown in Figure 8B. The lateral view profiles of fracture morphology of this artificial nacre nanocomposites are shown in Figure 8C. The edges of pulled-out graphene nanosheets show obvious substantial curling. Tensile strength and toughness can be simultaneously improved by this synergistic interaction of hydrogen and covalent bonding. This kind of artificial nacre nanocomposites have elastic and plastic properties, under cyclic loading-unloading testing, as shown in Figure 8D. Within a strain of 0.5% of Stage I, the artficial nacre nanocomposites show elastic behavior with reversible deformation, due to the weak hydrogen bonding. With increasing the tensile strain to 5% in Stage II, the artificial nacre nanocomposites show typical plastic behavior, resulting in a permanent deformationof 0.52% after five successive loading-unloading cycles, which may be due to broken of covalent bonds. In Stage III with a strain of 9%, the artificial nacre nanocomposites show large permanent deformation of 2.56% after five successive loading-unloading cycles. When the loading is further increased, the covalent bonding is completely broken, resulting in high fracture strength and curling of GO nanosheets. The proposed fracture mechanism is shown in Figure 8E. Firstly, the artficial nacre nanocomposites are stretched and the weak hydrogen bonds between adjacent graphene nanosheets break along with the slippage of graphene nanosheets. Then the coiled CS chains are stretched with increased loading. Finally, the covalent bondings between graphnene nanosheets and the CS chain are broken. This strategy of synergistic interactions of hydrogen and covalent bonding supplies a new avenue for the development of integrated high performance graphene-based artificial nacre nanocomposites.

3.2 Synergistic effect from building blocks

Incorporating the synergistic effect from building blocks is the other approach to achieve integrated graphene-based artificial nacre nanocomposites, which are inspired by natural nacre with 1D nanofibrillar chitin and 2D aragonite calcium carbonate platelets. In fact, recent studies on ternary nanocomposites with two different reinforcement components have revealed the importance of the synergistic effect from two building blocks, which simultaneously improves the tensile strength and toughness.[42, 43] For example, Prasad *et al.*[42] observed the synergistic effect from 1D carbon nanotubes and 2D graphene in the ternary nanocomposites based on the matrix of PVA. Then, Shin *et al.*[43] demonstrated ultratough ternary nanocomposites fiber with a synergistic toughening PVA matrix using rGO and single-walled carbon nanotubes. For the graphene-based artificial nacre nanocomposites, the second building blocks could be the ID nanofibers, such as carbon nanotubes, nanofibrillar, and 2D platelets, including nanoclay, disulphide (molybdenum disulfide, MoS_2 and tungsten disulfide, WS_2), et al. The synergistic effect from building blocks not only achieves integrated high tensile strength and toughness, but also introduces other functional properties for the resultant artificial nacre nanocomposites. In the following section, the synergistic effect from 1D and 2D building blocks with graphene nanosheets is explained in detail.

3.2.1 Combination with 1D building blocks

Gong *et al.*[44] demonstrated integrated strong, tough, and conductive ternary nanocomposites with a synergistic effect from rGO and double-walled carbon nanotubes (DWNTs). The schematic illustration of the assembly process is shown in

Figure 9A. The GO/DWNTs' homogeneous suspension was firstly assembled into GO-DWNTs hybrid layered materials via evaporation. Then, the linear PCDO molecules were grafted to GO nanosheets of the hybrid layered materials, and then were cross-linked by 1,4-addition polymerization of their diacetylenic units under UV irradiation. The residual groups on the GO nanosheets were removed with HI reduction. The cross-section of rGO-DWNTs-PCDO ternary nanocomposites is shown with the transmission electron microscopy image, revealing that the DWNT is attached on the surface of graphene nanosheets through π-π stacking. These ternary graphene-based nanocomposites show high mechanical properties with a tensile strength of 374.1 MPa and toughness of 9.2 MJ/m^3. Incorporation of DWNTs facilitates the electrical conductivity of ternary nanocomposites, resulting in 394.0 S/cm.

Furthermore, the synergistic effect from 1D DWNTs and 2D graphene nanosheets leads to extraordinary fatigue-resistant properties, as shown in Figure 9B. The fatigue life of the ternary nanocomposites is almost five orders of magnitude higher than that of binary GO-DWNT hybrid layered materials at the same stress level, which is attributed to the synergistic effect from 1D DWNTs and 2D GO nanosheets, and the covalent bonding between PCDO and GO nanosheets. Crack propagation was deflected by 2D GO nanosheets, resulting in an increase of fracture surface area during crack growth. Crack propagation was also suppressed by 1D DWNTs through crack bridging and a subsequent pull-out of DWNTs. In the ternary nanocomposites, the energy dissipation was synergistically enhanced by these two crack suppression mechanisms, leading to high fatigue life. The corresponding fracture morphologies of binary GO-DWNTs hybrid materials and ternary nanocomposites after fatigue testing are shown in Figures 9C and 9D, respectively. Obviously, the 1D DWNTs are curled much more than that of static mechanical testing, especially in ternary nanocomposites, which further confirms the crack-bridging abilities of 1D DWNTs for suppressing crack propagation. Compared with natural nacre and other graphene-based nanocomposites, this type of ternary nanocomposites shows advantages in tensile strength and toughness due to the synergistic toughening plus covalent bonding, as shown in Figure 9E.

3.2.2 Combination with 2D building blocks

2D molybdenum disulfide (MoS_2) nanosheets, an analogue of graphene, exhibit very good lubricant and high mechanical properties. The MoS_2 monolayer shows a tensile strength of about 23 GPa, Young's modulus of about 270 GPa, and a high tensile strain of 6-11%, all of which are comparable to those of chemically reduced graphene nanosheets. Thus, 2D MoS_2 also has been used as the reinforcing building block for polymer nanocomposites. MoS_2 is an ideal 2D building block for constructing the synergistic effect with GO nanosheets in artificial nacre nanocomposites. Wan *et al.*[45] demonstrated integrated strong and tough ternary artificial nacre nanocomposites through a synergistic effect from 2D MoS_2 and GO nanosheets. The mixture solution of GO, MoS_2, and thermoplastic polyurethane (TPU) was assembled into the ternary artificial nacre nanocomposites with vacuum-assisted filtration, as shown in Figure 10A. The tensile stress-strain curves demonstrated high mechanical properties of the ternary rGO-MoS_2-TPU nanocomposites, compared with binary rGO-TPU nanocomposites, as shown in Figure 10B.

On the other hand, the lubrication of MoS_2 in the ternary artificial nacre nanocomposites plays a key role in the synergistic toughening, and the critical amount of MoS_2 is optimized to be about 4 wt.% in the ternary artificial nacre nanocomposites. Below 4 wt.%, crack propagation cannot be effectively deflected. On the other hand, at higher than 4 wt.% the MoS_2 would form excessive restacking, leading to low efficiency of stress transfer between rGO and MoS_2 nanosheets. Wan *et al.*[45] proposed a crack extension model to explore the synergistic toughening effect from GO and MoS_2 nanosheets, as shown in Figure 10B. With increased loading, the weak hydrogen bonds between rGO nanosheets and TPU are broken first. Then, friction triggers the moving of MoS_2 along the rGO nanosheets, and crack propagation would be deflected by MoS_2 nanosheets with sliding between molybdenum and sulfur nanolayers due to the lubrication action from the 2H MoS_2. Thus, much energy would dissipate in the cycling of crack initiation-propagation-deflection until the ternary rGO-MoS_2-TPU nanocomposites fracture, leading to large strain. Finally, the damaged MoS_2 nanosheets were absorbed on the pulled-out rGO nanosheets, as shown in Figure 10C. This kind of synergistic effect results in an integrated tensile strength and toughness of ternary artificial nacre nanocomposites. For example, the tensile strength and toughness simultaneously reach 235 MPa and 6.9 MJ/m^3, respectively, which are superior to other common binary graphene-based materials.

Compared with lubrication of MoS_2 nanosheets, the other functional nanosheets can also be introduced to construct multifunctional integrated ternary graphene-based nanocomposites. For example, Ming *et al.*[46] fabricated multifunctional ternary artificial nacre nanocomposites of GO and montmorillonite (MMT) nanosheets with PVA via avacuum-assisted filtration self-assembly process. MMT nanosheets with excellent mechanical properties show unique fire retardant properties, and are also ideal candidates for constructing artificial nacre nanocomposites. After optimizing the ratio of MMT to GO nanosheets, an effective synergistic toughening effect was achieved, resulting in integrated strong and tough artificial nacre. The tensile strength and toughness reach 356.0 MPa and 7.5 MJ/m^3, respectively. Meanwhile, these ternary graphene-based artificial nacre nanocomposites show four orders of magnitude higher fatigue life than that of binary graphene-based artificial nacre nanocomposites, which may be attributed to the effective synergistic effect from graphene and MMT nanosheets. Furthermore, this ternary graphene-based artificial nacre nanocomposites also demonstrate high electrical conductivity with a maximum of 136.4 S/cm, higher than the ternary rGO-MoS_2-TPU nanocomposites. These multifunctional properties give this kind of ternary nanocomposites great potential for applications in the field of aerospace and for creating flexible electrodes in flexible devices. Meanwhile, due to the good fire retardant properties of MMT platelets, the ternary rGO-MMT-PVA nanocomposites show good fire retardant properties with only a small amount of MMT. For example, a silk cocoon placed behind this ternary rGO-MMT-PVA nanocomposites did not catch fire even upon prolonged exposure for 5 minutes to a high flame.

4. Guidelines for designing graphene-based artificial nacre nanocomposites

GO nanosheets with abundant functional groups are one of best building blocks for constructing high performance graphene-based artificial nacre nanocomposites. Meanwhile, GO nanosheets can be easily chemically reduced to graphene nanosheets. Thus, the other desired functional properties, including electrical and thermal conductivities, would be obtained together with mechanical properties, which are superior to other inorganic building blocks such as nanoclay, man-made $CaCO_3$ platelet, Al_2O_3 flake, et al. Herein, we propose two guidelines for designing high performance graphene-based artificial nacre nanocomposites: (i) constructing alternately order graphene nanosheets/organic matrix structure with the content of the organic matrix comparable to that of natural nacre. (ii) establishing interface interactions between graphene nanosheets and organic components. The comparison of mechanical properties of graphene-based artificial nacre nanocomposites with different interface interactions and synergistic effects is shown in Figure 11, and the detailed mechanical properties are listed in Table 1.

Covalent bonding dramatically enhances the mechanical properties of graphene-based artificial nacre nanocomposites compared with hydrogen bonding, ionic bonding, and π-π interactions, respectively, as show in the blue area. The mechanical properties of resultant nanocomposites are comparable to natural nacre. The synergistic effect plays a key role in further improving the mechanical properties of graphene-based artificial nacre nanocomposites, as shown in the pink area. Although the synergistic effect from interface interactions[41] in binary graphene-based artificial nacre nanocomposites is better for enhancing the mechanical properties, the synergistic effect from building blocks in ternary graphene-based artificial nacre nanocomposites also shows three advantages: (i) the unique functional properties can be incorporated with functional building blocks, for example, fatigue[43] and fire-retardant[45] properties; (ii) the synergistic effect could be quantifiably controlled through adjusting the ratios of building blocks; and (iii) much more complicated interface interactions could be constructed between graphene nanosheets with different building blocks to further improve the mechanical properties.

This tutorial review is mainly focused on the 2D graphene-based artificial nacre film nanocomposites. On the other hand, the 1D graphene-based fiber materials, firstly assembled by Gao *et al.*[47] in 2011, is also a promising graphene-based materials. Much more excellent mechanical and electrical properties of 1D graphene-based fiber have been achieved through interface design and interaction with different molecules, resulting in the promising applications, such as flexible wearable devices, and other functional materials, etc. Readers can refer recent an excellent review on the 1D graphene-based fiber materials.[47]

Table 1. The mechanical properties of natural nacre and other GO-based nanocomposites

		Nacre and artificial nacre	**Tensile strength (MPa)**	**Toughness (MJ/m^3)**	**Reference**
		Nacre	200.0	2.60	[9]
Interfacial interactions	Hydrogen bonding	GO-PVA	80.2	0.10	[18]
		GO-PMMA	148.3	2.35	[18]
		rGO-PVA	188.9	2.52	[19]
	Ionic bonding	GO-Ca^{2+}	125.8	0.31	[22]
		GO-Mg^{2+}	80.6	0.13	[22]
		GO-Al^{3+}	100.5	0.23	[23]
		GO-Zn^{2+}	142.2	0.32	[25]
	π-π interaction	rGO-PB	8.4	0.01	[26]
		rGO-FPEG	45.0	--	[29]
	Covalent bonding	GO-GA	101.0	0.30	[30]
		GO-Borate	185.0	0.14	[31]
		PGO-PEI	209.9	0.23	[32]
		rGO-PCDO	129.6	3.91	[34]
		GO-PAA	91.9	0.21	[35]
Synergistic effect	From hydrogen bonding, polar, and hydrophobic interactions	GO-SL	300.0	2.20	[36]
		rGO-SL	300.0	2.80	[37]

From π-πinteraction and hydrogen bonding	rGO-PAPB	382.0	7.50	[39]
From covalent and hydrogen bonding	rGO-PDA	204.9	4.00	[40]
	rGO-CS	526.7	17.69	[41]
From 1D building blocks	rGO-DWNT-PCDO	374.1	9.20	[44]
From 2D building blocks	rGO-MoS_2-TPU	235.0	6.90	[45]
	rGO-MMT-PVA	356.0	7.50	[46]

5. Applications

Graphene-based artificial nacre nanocomposites demonstrate integrated mechanical and electrical properties, and show great potential for applications in many fields, including electrical and energy devices, filters for separation, and intelligent devices such as generators and actuators, as shown in Figure 12. Goki *et al.*[48] firstly demonstrated rGO thin film with controllable thickness over large areas, and its optoelectronic properties can be tuned over six orders of magnitude and the transparencies from 60% to 95%, as shown in Figure 12A. The fabricated thin film transistors with reduced GO exhibit ambipolar characteristics at thin thickness. Furthermore, Goki *et al.*[49] fabricated transistors based on functionalized graphene sheets (FGS) and polystyrene. The transistor demonstrated ambipolar field effect characteristics and yielded the highest mobility values with the largest size FGS.

As shown in Figure 12B, graphene-based artificial nacre nanocomposites were designed as a photovoltaic device by Yu *et al*.[50] The device was assembled by CH_2OH-terminated regioregular poly(3-hexylthiophene) (P3HT) chemically grafted GO nanosheets through solution processing. The covalent linkage and the strong electronic interaction between the P3HT and graphene facilitate the structure/property characterization and the device fabrication by solution processing. The resultant bilayer photovoltaic device showed a 200% increase of the power conversion efficiency with respect to the P3HT/C_{60} counterpart under AM 1.5 illumination (100 mW/cm^2).

Maher *et al.*[51] fabricated a supercapacitor with electrodes of laser reduction of GO film that exhibited energy density values in different electrolytes and maintained high power density and outstanding cycle stability, as shown in Figure 12C. This kind of supercapacitor maintains extraordinary electrochemical attributes under high mechanical stress, showing promising applications in high-power and flexible electronics. Recently, Yang *et al.*[52] also demonstrated high performance flexible supercapacitors based on graphene gel nanocomposites. Highly compact carbon electrodes with a continuous ion transport network can be formed between graphene nanosheets and the nonvolatile liquid electrolyte, resulting in a supercapacitor with high volumetric energy densities approaching 60 watt-hours per liter.

Graphene-based artificial nacre nanocomposite is also the ideal candidate for constructing an actuator. For example, Yang *et al.*[53] demonstrated a superior and tunable photomechanical actuator based on graphene/liquid crystal elastomer (LCE) nanocomposites upon the exposure to NIR irradiation. These nanocomposites were judiciously yielded by combining the in situ UV photopolymerization of liquid-crystal mononers (LCMs) with the concurrent hot-stretching process, as shown in Figure 12D. The alignment of graphene nanosheets in the LCE matrix plays an important role of being a photoactive constituent. Meanwhile, the efficient interface interactions of π-π stacking between LC aromatic rings and graphene, and the hydrogen bonding between the hydroxyl and carboxyl groups in graphene and the ester groups in LCMs and the resulting LCEs, also plays an important role. Furthermore, the two distinct advantages of LCEs, that is, their self-organizing nature and entropy-driven elasticity, further enable larger reversible deformations of graphene/LCEs nanocomposites compared with conventional polymer nanocomposites.

A graphene-based hydrogel nanocomposite was developed as an integrated 2D nanofluidic generator by Guo *et al.*[54] as shown in Figure 12E. In wet conditions, a large-scale interconnected 2D nanofluidic network was formed all over the graphene hydrogel nanocomposites. The negatively charged 2D nanocapillaries formed between adjacent graphene nanosheets showed surface charge governed ion transportation that permeates counter-ions and excludes co-ions. An electrokinetic phenomenon was discovered when electrolyte flow vertically goes through the graphene hydrogel nanocomposites driven by external mechanical force. Continuous and pulse-shaped ionic current signals were received from the graphene hydrogel nanocomposites depending on the input wave induced by external mechanical force. These kinds of bioinspired design principles are applicable to other 2D layered materials for functional nanofluidic devices.

Huang *et al.*[55] developed superior separation performance filter-based nanostrand-channelled graphene materials, as shown in Figure 12F. The network of nanochannels with a narrow size distribution results in high filter permeance of 10-fold enhancement without sacrificing the rejection rate. The porous structure and reduced channel length play a key role in flow enhancement. Meanwhile, tunable permeation and rejection were realized through elastic deformation of nanochannels. And this nanostrand-channelling approach offers promising design concepts for other laminate membranes for accelerating separation and water-purification processes.

6. Conclusions and outlook

As predicted by Geim and Novoselov in 2007, one of the areas where graphene would shine in the future is composite materials.[2] Indeed, the papers describing various graphene-based nanocomposites are being published almost daily. This tutorial review summarizes recent research on graphene-based artificial nacre-like nanocomposites and discusses their different interface interactions. Four representative interface interactions, including hydrogen bonding, ionic bonding, π-π interactions, and covalent bonding, are discussed in detail. The influence of such synergistic effects resulting from the interface interactions and building blocks on mechanical properties of nacre-inspired nanocomposites is also discussed in detail. Synergistic interface interactions are better for further improvement of the mechanical properties of graphene-based nanocomposites as compared with the synergistic effect arising only from the building blocks. These interactions would provide additional functions, such as better fatigue and fire-retardant properties. By comparing the mechanical properties of several graphene-based nacre-inspired nanocomposites, two guidelines for assembling them are proposed: (i) graphene nanosheets/organic matrix, with the content of the organic matrix comparable to that of natural nacre, should be constructed as an alternating layered structure, (ii) the interface interactions between graphene nanosheets and organic components should be established. The integrated multifunctional graphene-based nanocomposites are being considered for several practical applications, including electrical and energy devices, filters for separation, and intelligent devices such as generators and actuators. These high performance bioinspired nanocomposites could be achieved through constructing different interfacial interactions and synergistic effects. Due to graphene's intrinsic 2D structure, a breakthrough in integrated multifunctional graphene-based artificial nacre nanocomposites with isotropic mechanical and electrical properties is anticipated in the near future.

In fact, although the great progress on the graphene-based artificial nacre nanocomposites have been achieved, there are still many challenges and issues needing to be solved for the practical applications of graphene-based nanocomposites, such as the large-scale fabrication approaches, well-designed hierarchical structure method, etc. In addition, the other big challenge is to find an effective way to tailor graphene surface chemistry and nanocomposite architecture for specific applications. The graphene research has now reached a stage where an innovative method of processing graphene nanocomposites to produce novel hybrid structures with remarkable properties is urgently needed.

Author Contributions

Y.Y. Zhang, S.S. Gong, Qi Zhang, P. Ming, S.J. Wan, J.S. Peng, L. Jiang and Q.F. Cheng, collected data from the references. L. Jiang and Q.F. Cheng discussed and analyzed the data. Y.Y. Zhang and Q. F. Cheng wrote the paper.

Acknowledgements

This work was supported by the Excellent Young Scientist Foundation of NSFC (51522301), the National Natural Science Foundation of China (21273017, 51103004), the Program for New Century Excellent Talents in University (NCET-12-0034), the Beijing Nova Program (Z121103002512020), the Fok Ying-Tong Education Foundation (141045), the Open Project of Beijing National Laboratory for Molecular Sciences, the 111 Project (B14009), the Aeronautical Science Foundation of China (20145251035, 2015ZF21009), the State Key Laboratory for Modification of Chemical Fibers and Polymer Materials, Donghua University (LK1508), and the Fundamental Research Funds for the Central Universities (YWF-15-HHXY-001).

References

1. K. S. Novoselov, V. I. Falko, L. Colombo, P. R. Gellert, M. G. Schwab and K. Kim, *Nature*, 2012, **490**, 192-200.
2. A. K. Geim and K. S. Novoselov, *Nat. Mater.*, 2007, **6**, 183-191.
3. X. Huang, X. Qi, F. Boey and H. Zhang, *Chem. Soc. Rev.*, 2012, **41**, 666-686.
4. R. J. Young, I. A. Kinloch, L. Gong and K. S. Novoselov, *Compos. Sci. Technol.*, 2012, **72**, 1459-1476.
5. D. Wu, F. Zhang, H. Liang and X. Feng, *Chem. Soc. Rev.*, 2012, **41**, 6160-6177.
6. M. Yang, Y. Hou and N. A. Kotov, *Nano Today*, 2012, **7**, 430-447.
7. X. Sun, H. Sun, H. Li and H. Peng, *Adv. Mater.*, 2013, **25**, 5153-5176.
8. K. Hu, D. D. Kulkarni, I. Choi and V. V. Tsukruk, *Prog. Polym. Sci.*, 2014, **39**, 1934-1972.
9. U. G. K. Wegst, H. Bai, E. Saiz, A. P. Tomsia and R. O. Ritchie, *Nat. Mater.*, 2015, **14**, 23-36.
10. H.-B. Yao, J. Ge, L.-B. Mao, Y.-X. Yan and S.-H. Yu, *Adv. Mater.*, 2014, **26**, 163-188.
11. H.-B. Yao, H.-Y. Fang, Z.-H. Tan, L.-H. Wu and S.-H. Yu, *Angew. Chem., Int. Ed.*, 2010, **49**, 2140-2145.

12. H.-B. Yao, Z.-H. Tan, H.-Y. Fang and S.-H. Yu, *Angew. Chem., Int. Ed.*, 2010, **49**, 10127-10131.
13. H.-P. Cong, J.-F. Chen and S.-H. Yu, *Chem. Soc. Rev.*, 2014, **43**, 7295-7325.
14. M. A. Meyers, J. McKittrick and P. Y. Chen, *Science*, 2013, **339**, 773-779.
15. E. Munch, M. E. Launey, D. H. Alsem, E. Saiz, A. P. Tomsia and R. O. Ritchie, *Science*, 2008, **322**, 1516-1520.
16. D. A. Dikin, S. Stankovich, E. J. Zimney, R. D. Piner, G. H. B. Dommett, G. Evmenenko, S. T. Nguyen and R. S. Ruoff, *Nature*, 2007, **448**, 457-460.
17. N. V. Medhekar, A. Ramasubramaniam, R. S. Ruoff and V. B. Shenoy, *ACS Nano*, 2010, **4**, 2300-2306.
18. K. W. Putz, O. C. Compton, M. J. Palmeri, S. T. Nguyen and L. C. Brinson, *Adv. Funct. Mater.*, 2010, **20**, 3322-3329.
19. Y.-Q. Li, T. Yu, T.-Y. Yang, L.-X. Zheng and K. Liao, *Adv. Mater.*, 2012, **24**, 3426-3431.
20. O. C. Compton, S. W. Cranford, K. W. Putz, Z. An, L. C. Brinson, M. J. Buehler and S. T. Nguyen, *ACS Nano*, 2012, **6**, 2008-2019.
21. S. M. Lee, E. Pippel, U. Gosele, C. Dresbach, Y. Qin, C. V. Chandran, T. Brauniger, G. Hause and M. Knez, *Science*, 2009, **324**, 488-492.
22. S. Park, K.-S. Lee, G. Bozoklu, W. Cai, S. T. Nguyen and R. S. Ruoff, *ACS Nano*, 2008, **2**, 572-578.
23. C.-N. Yeh, K. Raidongia, J. Shao, Q.-H. Yang and J. Huang, *Nat. Chem.*, 2015, **7**, 166-170.
24. X. Jiang, Y. Ma, J. Li, Q. Fan and W. Huang, *J. Phys. Chem. C*, 2010, **114**, 22462-22465.
25. D. V. Lam, T. Gong, S. Won, J. H. Kim, H. J. Lee, C. Lee and S. M. Lee, *Chem. Commun.*, 2015, **51**, 2671-2674.
26. Y. Xu, H. Bai, G. Lu, C. Li and G. Shi, *J. Am. Chem. Soc.*, 2008, **130**, 5856-5857.
27. Y. Liu, L. Yuan, M. Yang, Y. Zheng, L. Li, L. Gao, N. Nerngchamnong, C. T. Nai, C. S. S. Sangeeth, Y. P. Feng, C. A. Nijhuis and K. P. Loh, *Nat. Commun.*, 2014, **5**, 6461-6468.
28. C.-C. Teng, C.-C. M. Ma, C.-H. Lu, S.-Y. Yang, S.-H. Lee, M.-C. Hsiao, M.-Y. Yen, K.-C. Chiou and T.-M. Lee, *Carbon*, 2011, **49**, 5107-5116.
29. J. Zhang, Y. Xu, L. Cui, A. Fu, W. Yang, C. Barrow and J. Liu, *Compos. Part. A-Appl. S*, 2015, **71**, 1-8.

30. Y. Gao, L.-Q. Liu, S.-Z. Zu, K. Peng, D. Zhou, B.-H. Han and Z. Zhang, *ACS Nano*, 2011, **5**, 2134-2141.
31. Z. An, O. C. Compton, K. W. Putz, L. C. Brinson and S. T. Nguyen, *Adv. Mater.*, 2011, **23**, 3842-3846.
32. Y. Tian, Y. Cao, Y. Wang, W. Yang and J. Feng, *Adv. Mater.*, 2013, **25**, 2980-2983.
33. Z. Jia and Y. Wang, *J. Mater. Chem. A*, 2015, **3**, 4405-4412.
34. Q. Cheng, M. Wu, M. Li, L. Jiang and Z. Tang, *Angew. Chem., Int. Ed.*, 2013, **52**, 3750-3755.
35. S. Park, D. A. Dikin, S. T. Nguyen and R. S. Ruoff, *J. Phys. Chem. C*, 2009, **113**, 15801-15804.
36. K. Hu, M. K. Gupta, D. D. Kulkarni and V. V. Tsukruk, *Adv. Mater.*, 2013, **25**, 2301-2307.
37. K. Hu, L. S. Tolentino, D. D. Kulkarni, C. Ye, S. Kumar and V. V. Tsukruk, *Angew. Chem., Int. Ed.*, 2013, **52**, 13784-13788.
38. C. Li and G. Q. Shi, *Adv. Mater.*, 2014, **26**, 3992-4012.
39. M. Zhang, L. Huang, J. Chen, C. Li and G. Shi, *Adv. Mater.*, 2014, **26**, 7588-7592.
40. W. Cui, M. Li, J. Liu, B. Wang, C. Zhang, L. Jiang and Q. Cheng, *ACS Nano*, 2014, **8**, 9511-9517.
41. S. Wan, J. Peng, Y. Li, H. Hu, L. Jiang and Q. Cheng, *ACS Nano*, 2015, **9**, 9830-9836.
42. K. E. Prasad, B. Das, U. Maitra, U. Ramamurty and C. N. R. Rao, *Proc. Natl. Acad. Sci. U.S.A.*, 2009, **106**, 13186-13189.
43. M. K. Shin, B. Lee, S. H. Kim, J. A. Lee, G. M. Spinks, S. Gambhir, G. G. Wallace, M. E. Kozlov, R. H. Baughman and S. J. Kim, *Nat. Commun.*, 2012, **3**, 650-657.
44. S. Gong, W. Cui, Q. Zhang, A. Cao, L. Jiang and Q. Cheng, *ACS Nano*, 2015, **9**, 11568-11573.
45. S. Wan, Y. Li, J. Peng, H. Hu, Q. Cheng and L. Jiang, *ACS Nano*, 2015, **9**, 708-714.
46. P. Ming, Z. Song, S. Gong, Y. Zhang, J. Duan, Q. Zhang, L. Jiang and Q. Cheng, *J. Mater. Chem. A*, 2015, **3**, 21194-21200.
47. Z. Xu and C. Gao, *Acc. Chem. Res.*, 2014, **47**, 1267-1276.

48. G. Eda, G. Fanchini and M. Chhowalla, *Nat Nano*, 2008, **3**, 270-274.

49. G. Eda and M. Chhowalla, *Nano Lett.*, 2009, **9**, 814-818.

50. D. S. Yu, Y. Yang, M. Durstock, J. B. Baek and L. M. Dai, *ACS Nano*, 2010, **4**, 5633-5640.

51. M. F. El-Kady, V. Strong, S. Dubin and R. B. Kaner, *Science*, 2012, **335**, 1326-1330.

52. X. Yang, C. Cheng, Y. Wang, L. Qiu and D. Li, *Science*, 2013, **341**, 534-537.

53. Y. Yang, W. Zhan, R. Peng, C. He, X. Pang, D. Shi, T. Jiang and Z. Lin, *Adv. Mater.*, 2015, **27**, 6376-6381.

54. W. Guo, C. Cheng, Y. Wu, Y. Jiang, J. Gao, D. Li and L. Jiang, *Adv. Mater.*, 2013, **25**, 6064-6068.

55. H. Huang, Z. Song, N. Wei, L. Shi, Y. Mao, Y. Ying, L. Sun, Z. Xu and X. Peng, *Nat. Commun.*, 2013, **4**, 3979-3987.

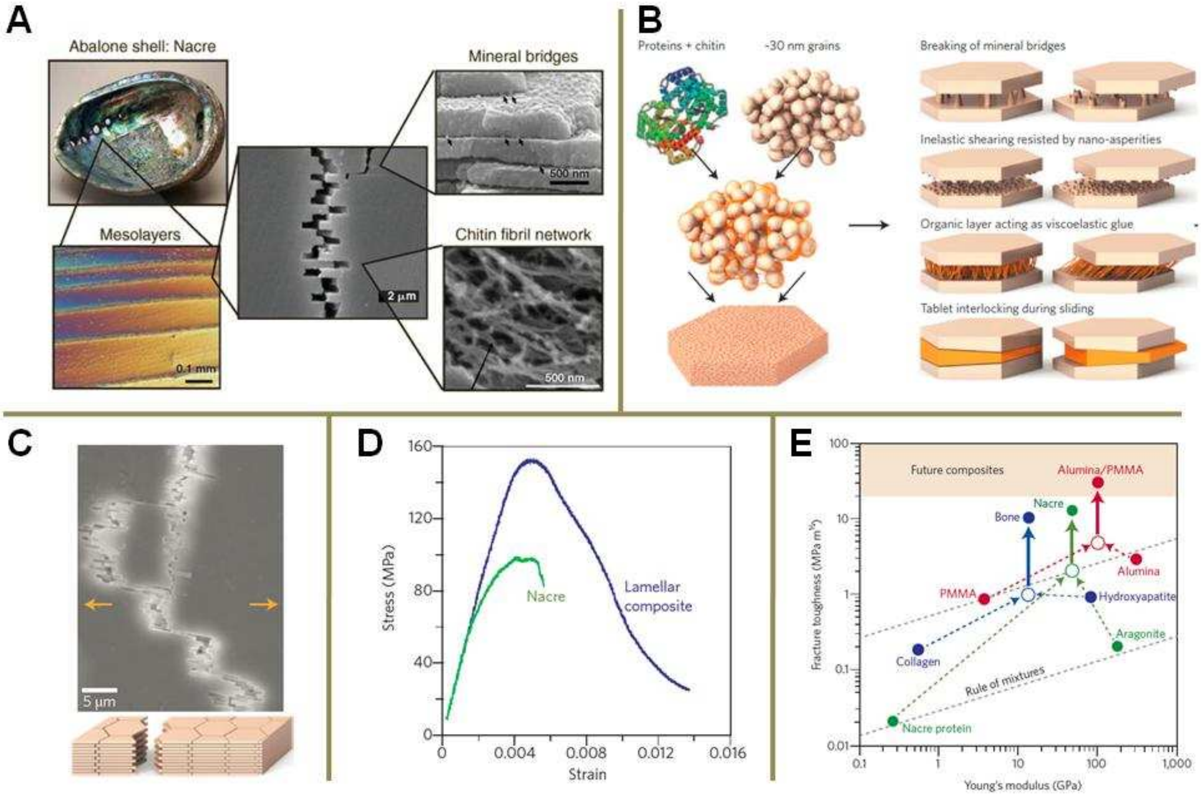

Figure 1. (A) Nacre shows orderly layered structure with inorganic $CaCO_3$ platelets and organic layer, which contains the biopolymer and fibrous chitin network. Reproduced from ref. 14 with permission from Copyright 2013 The American Association for the Advancement of Science. (B) Nanograins are assembled into the aragonite platelets with glue of biopolymers; the micro-scale aragonite platelets promote four kinds of interface interactions: (i) mineral bridges between $CaCO_3$ platelets; (ii) nano-asperities for shearing resistance; (iii) organic glue; and (iv) tablet interlocking. (C) Crack propagation in natural nacre is deflected around the orderly layered structure, dissipating much more energy (orange arrows show the direction of tension). Reproduced from ref. 9 with permission from Copyright 2014 Nature Publishing Group. (D) Bending strength comparison of nacre and nacre-mimetic lamellar composites of Al_2O_3/PMMA ceramic materials. Reproduced from ref. 15 with permission from Copyright 2008 The American Association for the Advancement of Science. (E) Natural nacre shows high toughness, far exceeding that of its constituents and its homogeneous mixtures. Reproduced from ref. 9 with permission from Copyright 2014 Nature Publishing Group.

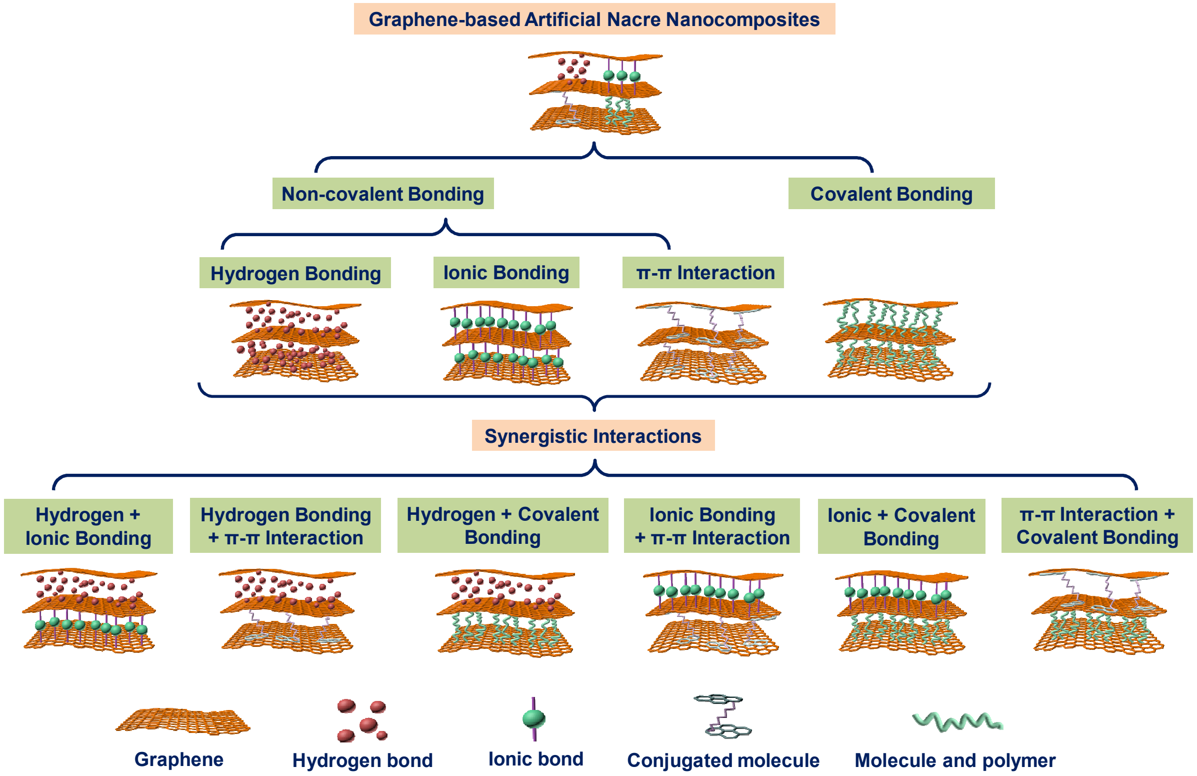

Figure 2. The interface interactions design for graphene-based artificial nacre nanocomposites, which can be categorized into two classes: (i) non-covalent bonding and (ii) covalent bonding. The non-covalent bonding mainly contains hydrogen bonding, ionic bonding, and π-π interaction. Any two different interface interactions can be combined together, resulting in synergistic effect for improving the performance of graphene-based artificial nacre nanocomposites.

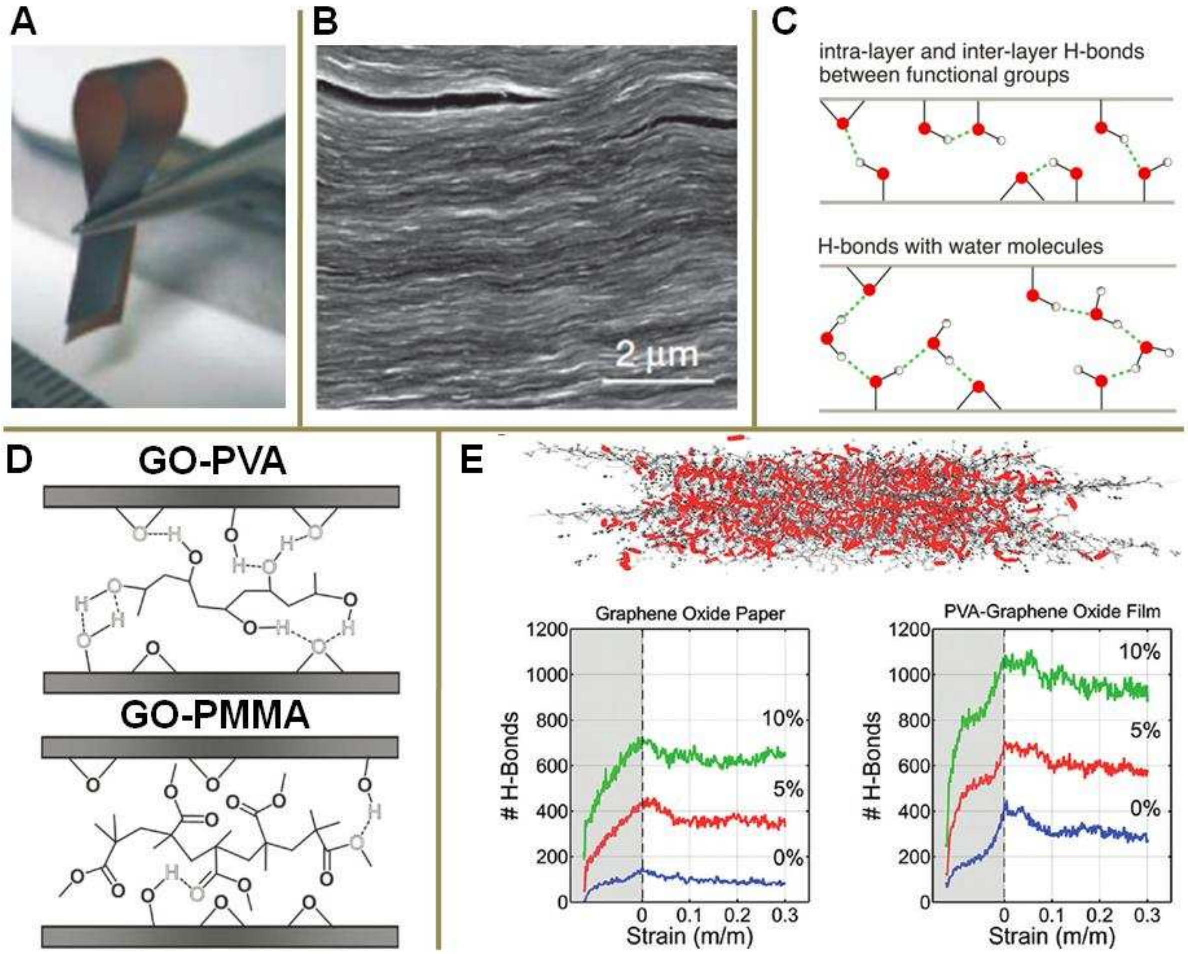

Figure 3. Hydrogen bonding in the graphene-based artificial nacre nanocomposites. (A) Photos of GO paper with thickness of 5 μm. Reproduced from ref. 16 with permission from Copyright 2007 Nature Publishing Group. (B) Cross-section surface morphology of GO paper. Reproduced from ref. 16 with permission from Copyright 2007 Nature Publishing Group. (C) Schematic illustration of various configurations of hydrogen bonding between GO nanosheets and with the water molecules. Reproduced from ref. 17 with permission from Copyright 2010 American Chemical Society. (D) Hydrogen bonding between GO nanosheets with PVA and PMMA chains, respectively. Reproduced from ref. 18 with permission from Copyright 2010 Wiley-VCH. (E) Model snapshot for the hydrogen bonding network in GO-PVA nanocomposites, and plots depicting the total number of hydrogen bonding as a function of applied strain in GO paper and GO-PVA nanocomposites. Reproduced from ref. 20 with permission from Copyright 2012 American Chemical Society.

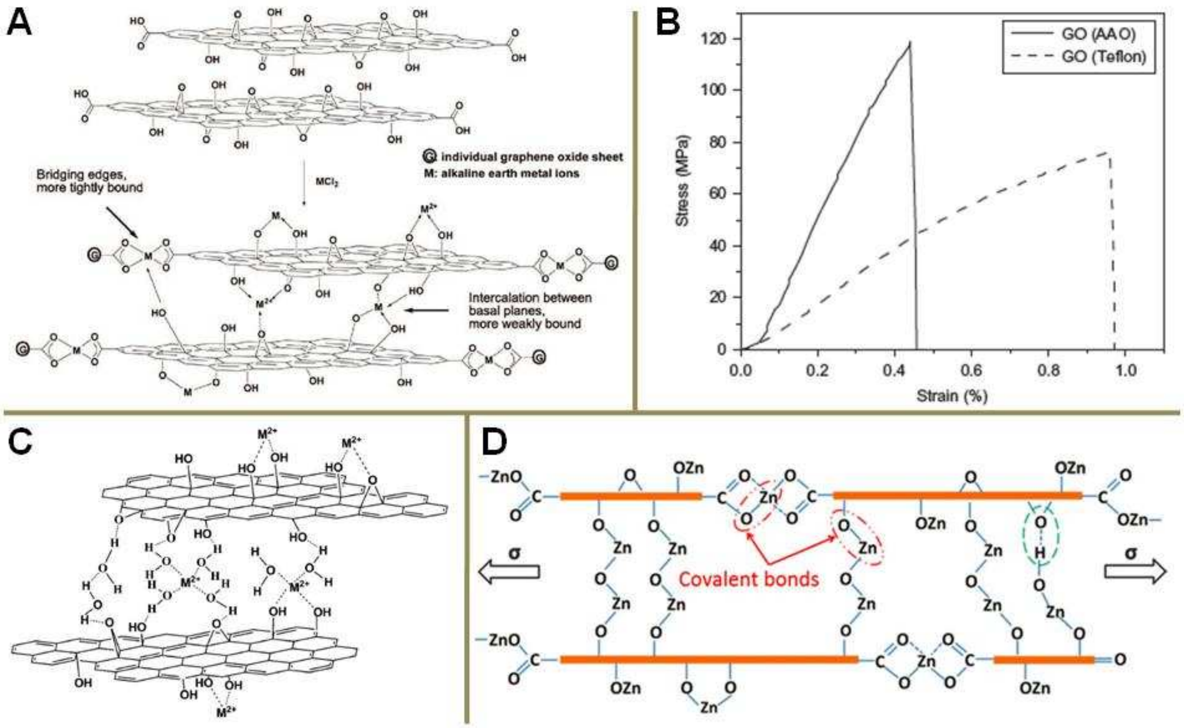

Figure 4. Ionic bonding in the graphene-based artificial nacre nanocomposites. (A) Proposed model of metal ion bonding of Mg^{2+} and Ca^{2+} with GO nanosheets. Reproduced from ref. 22 with permission from Copyright 2008 American Chemical Society. (B) Comparison of tensile stress between Al^{3+} cross-linked GO (AAO) paper with pure GO (Teflon) paper. Reproduced from ref. 23 with permission from Copyright 2015 Nature Publishing Group. (C) Schematic illustration of divalent ion (Ca^{2+}, Ni^{2+}, and Co^{2+}) linkage with GO nanosheets. Reproduced from ref. 24 with permission from Copyright 2010 American Chemical Society. (D) Proposed molecular structure changes for Zn^{2+} cross-linked GO nanosheets under stretching. Reproduced from ref. 25 with permission from Copyright 2014 Royal Society of Chemistry.

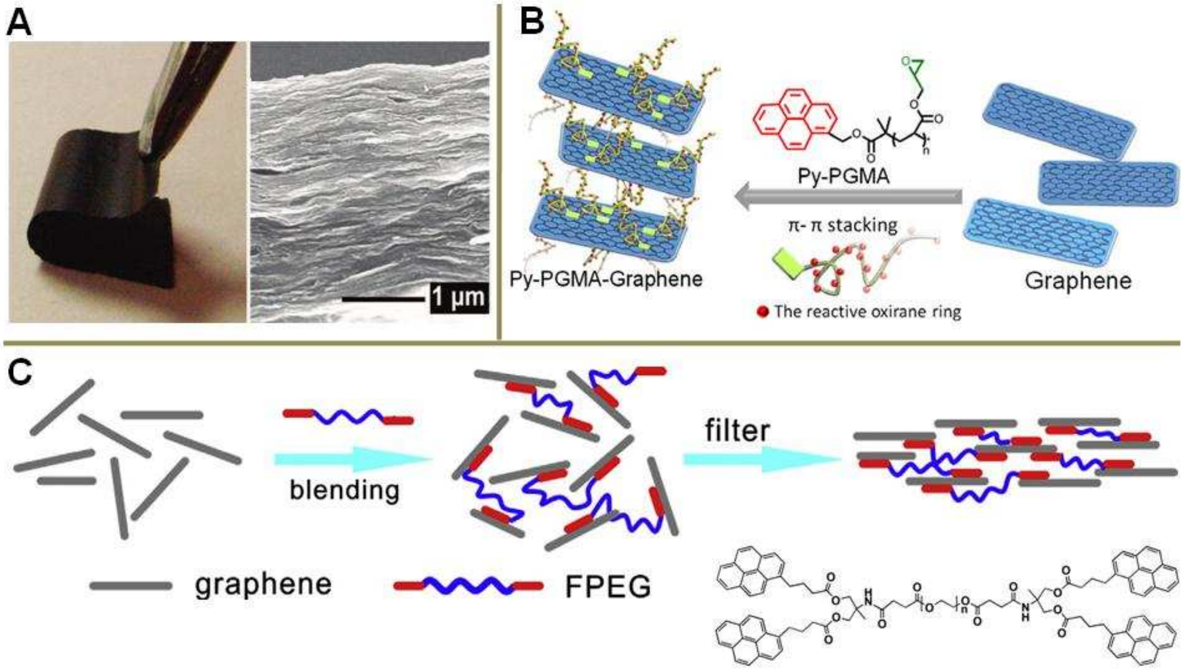

Figure 5. π-π interaction in the graphene-based artificial nacre nanocomposites. (A) Photograph and cross-section morphology of graphene-based nanocomposites cross-linked π-π interaction between graphene nanosheets with PB. Reproduced from ref. 26 with permission from Copyright 2008 American Chemical Society. (B) Poly(glycidyl methacrylate) containing localized pyrene groups (Py-PGMA) attached on graphene nanosheets through π-π interaction. Reproduced from ref. 28 with permission from Copyright 2011 Elsevier. (C) Schematic illustration of cross-linking graphene nanosheets by π-π interaction with FPEGs into the nanocomposites. Reproduced from ref. 29 with permission from Copyright 2015 Elsevier.

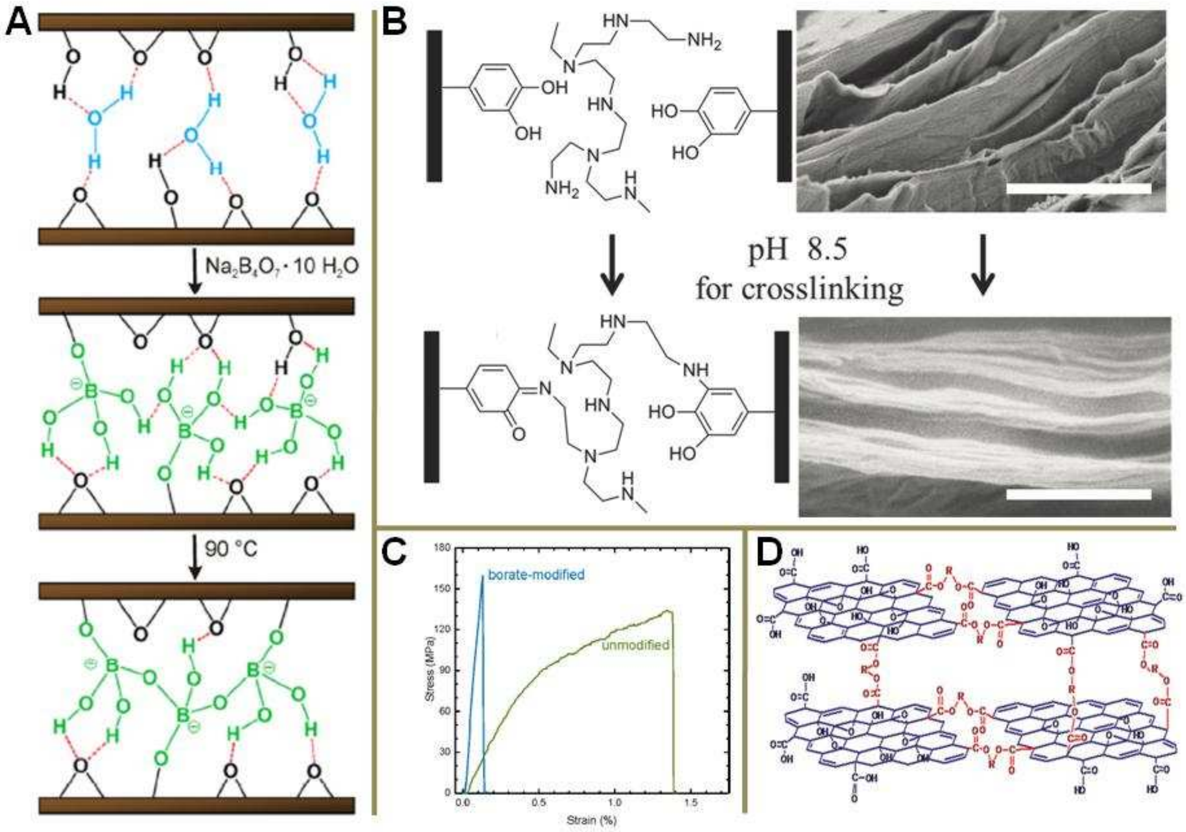

Figure 6. High strength and stiffness introduced from covalent bonding. (A) Formation process of covalent bonding between borate and GO nanosheets. Reproduced from ref. 31 with permission from Copyright 2011 Wiley-VCH. (B) Schematic illustration of covalent cross-linking adjacent PDA grafted GO nanosheets with PEI. Reproduced from ref. 32 with permission from Copyright 2013 Wiley-VCH. (C) Stress-strain curves comparison of the unmodified and borate cross-linked GO film. Reproduced from ref. 31 with permission from Copyright 2011 Wiley-VCH. (D) Proposed covalent bonding between GO nanosheets and diols (HO–R–OH). Reproduced from ref. 33 with permission from Copyright 2015 Royal Society of Chemistry.

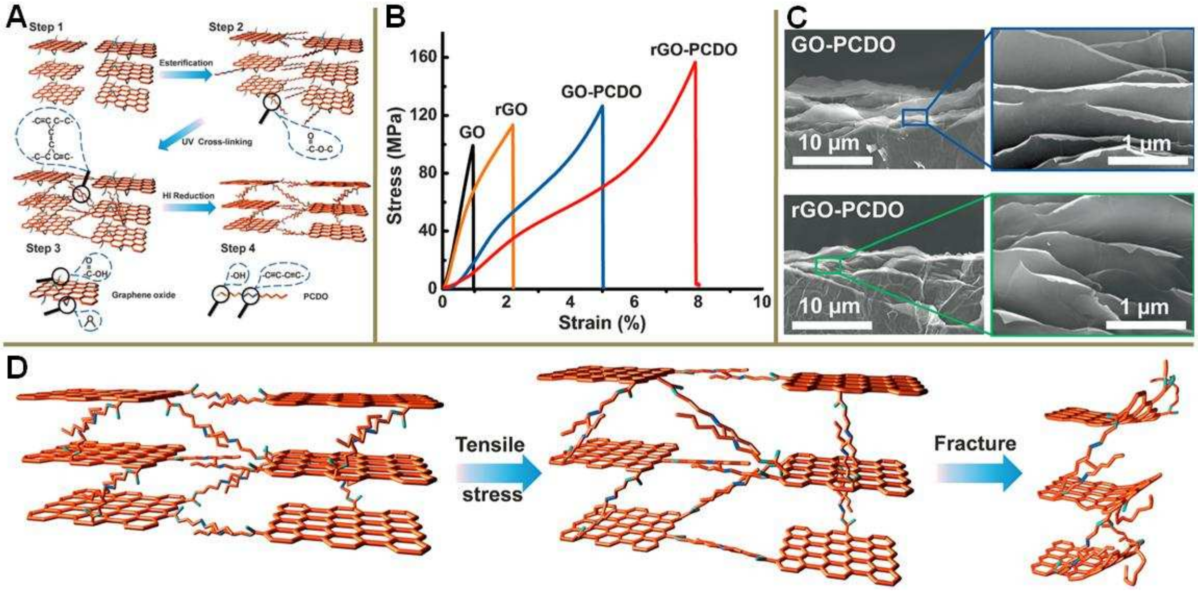

Figure 7. High toughness introduced from covalent bonding. (A) Schematic illustration of long chain molecule 10,12-pentacosadiyn-1-ol (PCDO) cross-linking adjacent GO nanosheets. (B) Tensile stress-strain curves of GO film and GO-PCDO nanocomposites. (C) Fracture morphology of GO-PCDO and rGO-PCDO nanocomposites indicates the edge curving of graphene nanosheets after breaking of chemical bonds between graphene nanosheets with PCDO. (D) Proposed corresponding fracture mechanism of rGO-PCDO nanocomposites. Reproduced from ref. 34 with permission from Copyright 2013 Wiley-VCH.

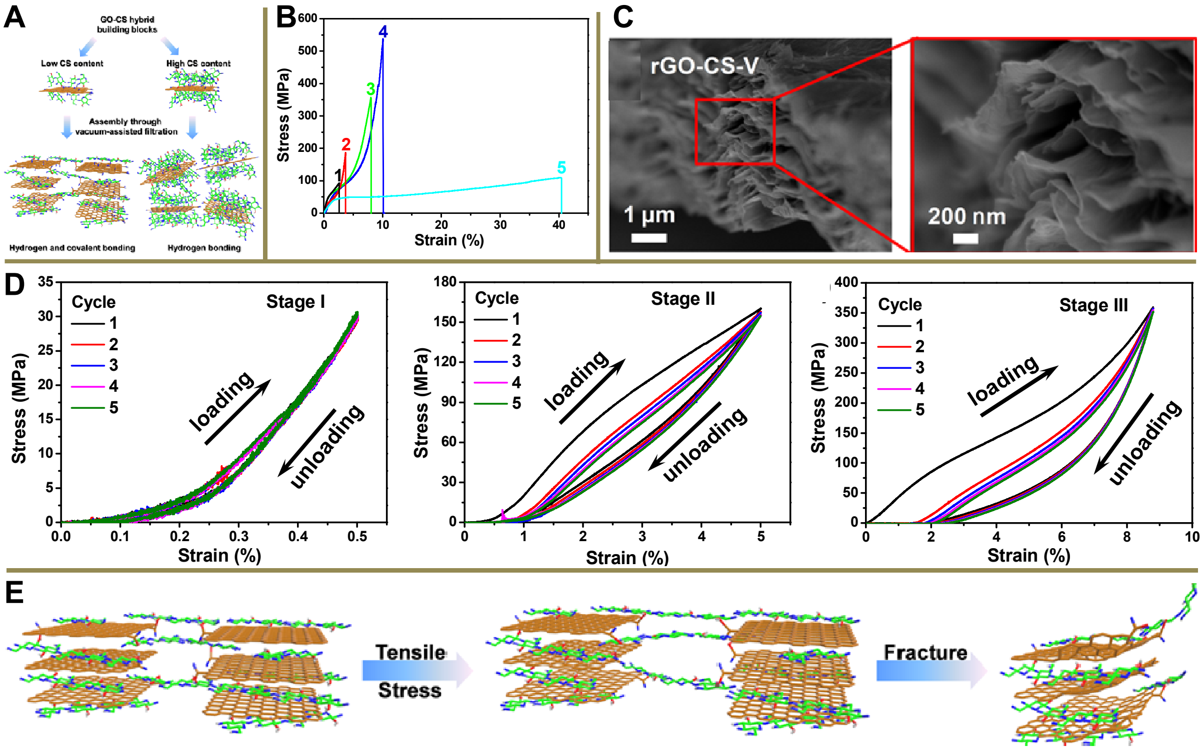

Figure 8. Synergistic effect from covalent and hydrogen bonding. (A) Proposed mechanism of synergistic interactions between CS and GO nanosheets. (B) Tensile stress-strain curves comparison of CS film, GO film, and CS-GO nanocomposites. (C) Lateral view profiles of fractured morphology of graphene-based artificial nacre nanocomposites. (D) Tensile stress-strain curves of graphene-based artificial nacre nanocomposites under cyclic loading-unloading tests: Stages I, II, and III represent the strain of 0.5%, 5%, and 9%, respectively. (E) Schematic illustration of fracture mechanism of graphene-based artificial nacre nanocomposites. Reproduced from ref. 41 with permission from Copyright 2015 American Chemical Society.

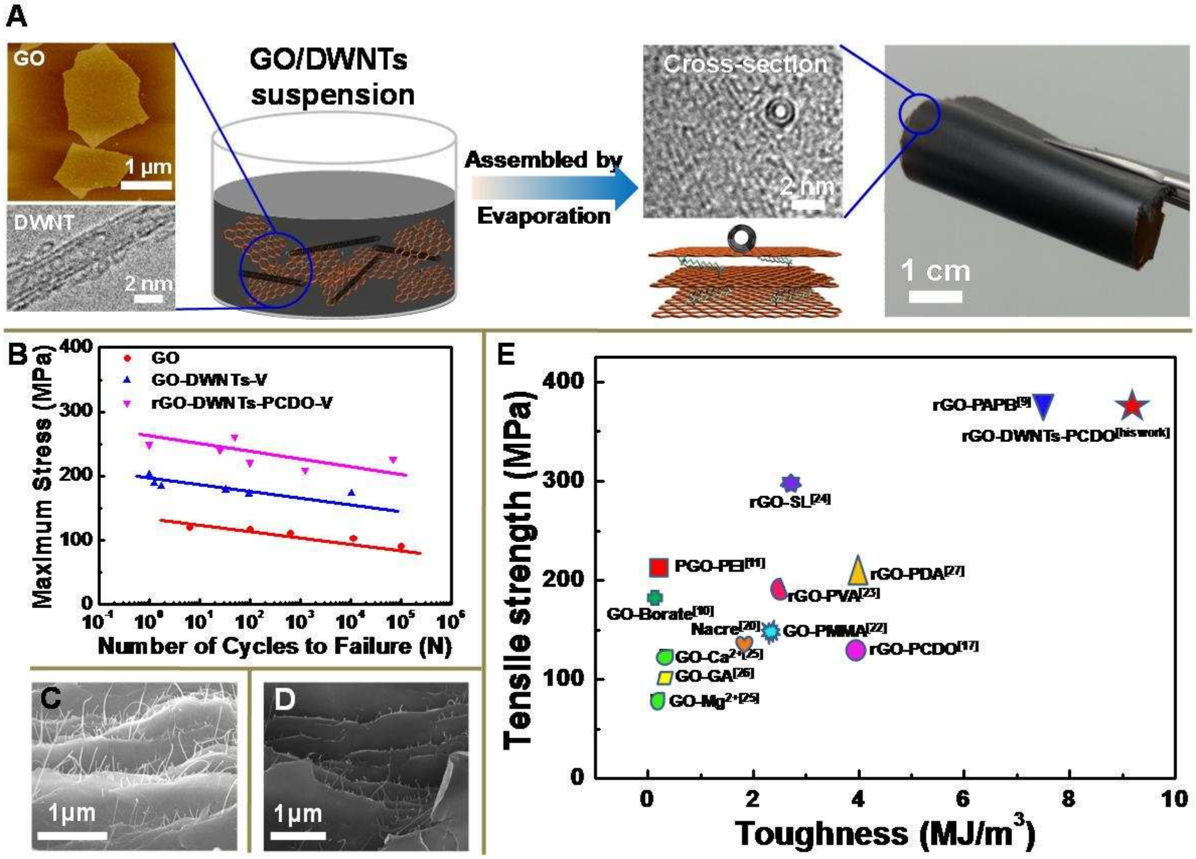

Figure 9. Synergistic effect from ID DWNTs and GO nanosheets. (A) Schematic illustration of the fabrication process for ternary artificial nacre nanocomposites. (B) Comparison of tensile fatigue testing between GO film, GO-DWNT binary nanocomposite, and rGO-DWNT-PCDO ternary nanocomposites. (C) and (D) Fracture morphology of GO-DWNT binary nanocomposite and rGO-DWNT-PCDO ternary nanocomposites after tensile fatigue testing. (E) Mechanical properties comparison with natural nacre and other binary GO-based nanocomposites. Reproduced from ref. 44 with permission from Copyright 2015 American Chemical Society.

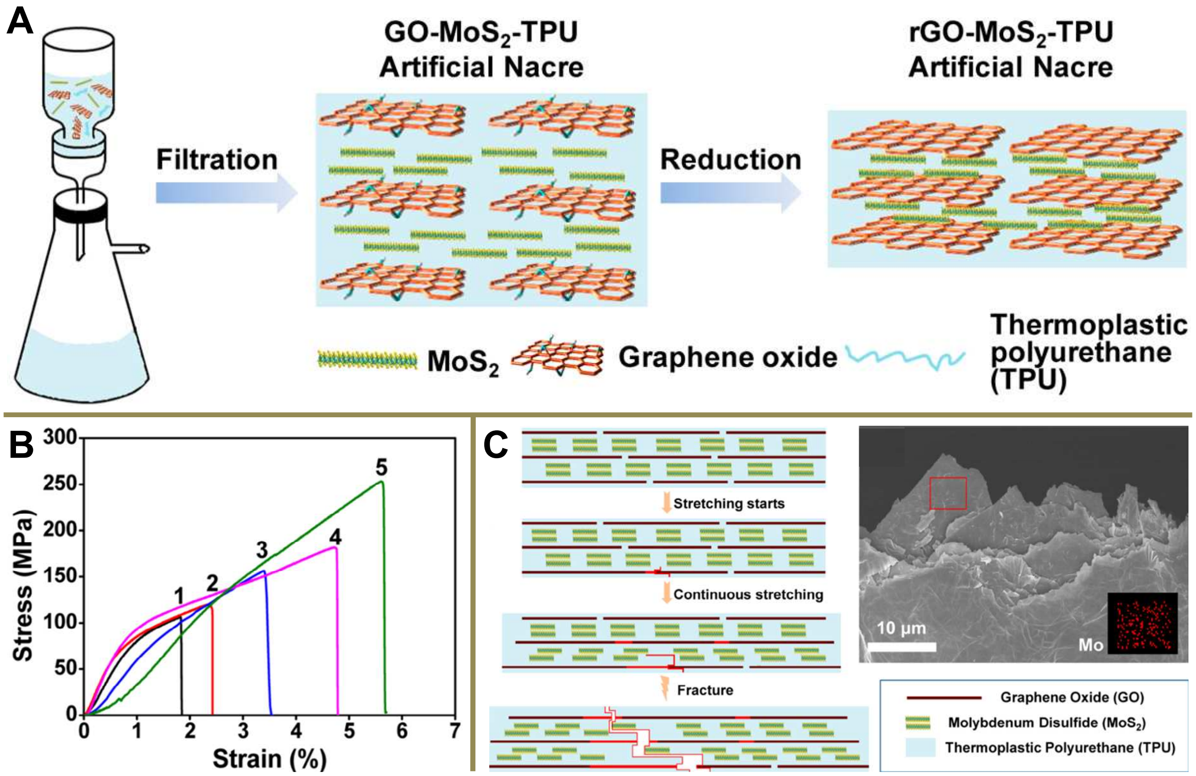

Figure 10. Synergistic effect from 2D MoS$_2$ and GO nanosheets. (A) Schematic illustration of preparation process of graphene oxide–molybdenum disulfide–TPU ternary artificial nacre nanocomposites. (B) Tensile stress-strain curves of GO film (curve 1), GO-TPU (curve 2), rGO-TPU (curve 3) binary and GO-MoS$_2$-TPU (curve 4), rGO-MoS$_2$-TPU (curve 5) ternary nanocomposites. (C) Proposed synergistic fracture mechanism and corresponding fracture morphology of rGO-MoS$_2$-TPU ternary nanocomposites. Reproduced from ref. 45 with permission from Copyright 2015 American Chemical Society.

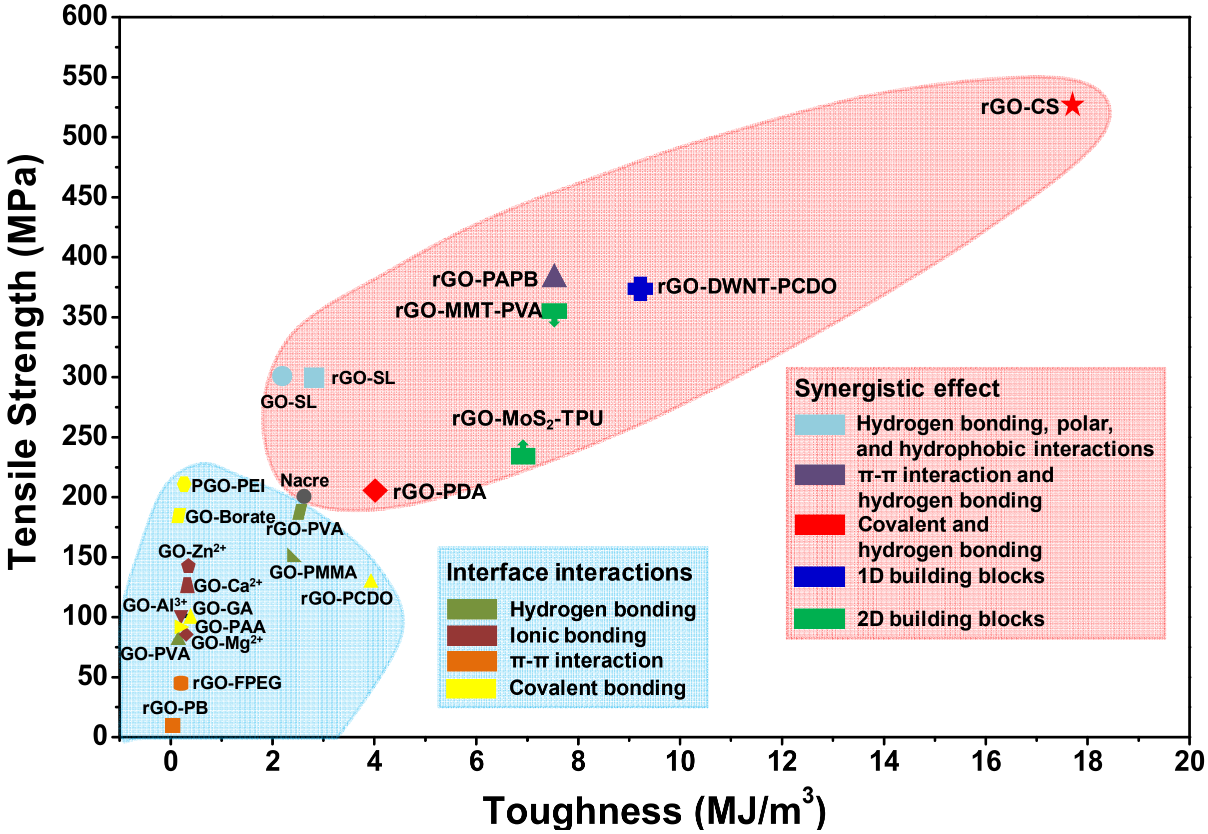

Figure 11. Mechanical properties comparison of natural nacre and graphene-based artificial nacre nanocomposites with different interface interactions and synergistic effects. The results show that covalent bonding is much more efficient for improving the mechanical properties of graphene-based artificial nacre nanocomposites than the other interface interactions including hydrogen bonding, ionic bonding and π-π interaction. In addition, the synergistic effect can dramatically improve the mechanical properties, especially for the synergistic effect from interface interactions.

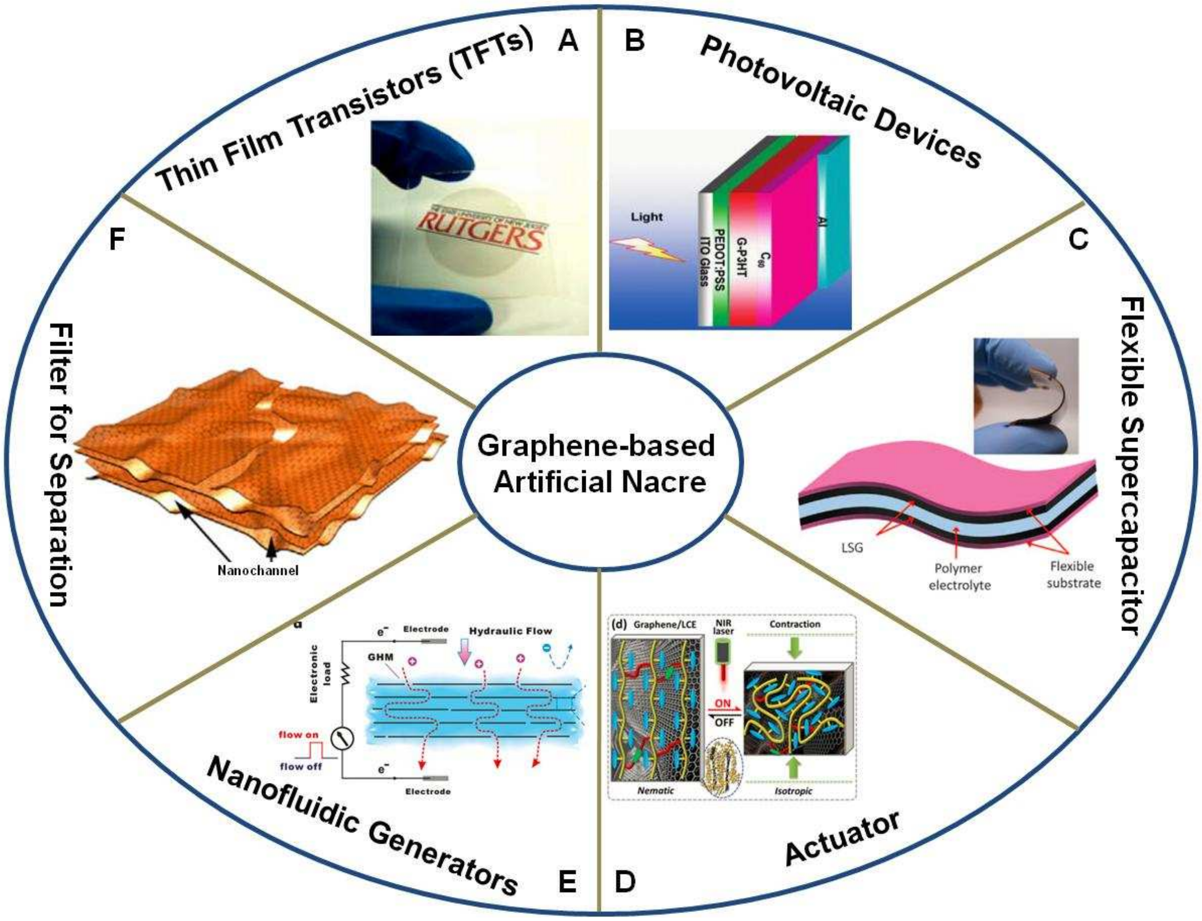

Figure 12. Applications of graphene-based artificial nacre nanocomposites: (A) Large-area ultrathin films of rGO as a transparent and flexible electronic material for the application of thin film transistors. Reproduced from ref. 48 with permission from Copyright 2008 Nature Publishing Group. (B) Bilayer regioregular poly(3-hexylthiophene) (P3HT)-grafted graphene nanocomposites for high performance heterojunction photovoltaic devices. Reproduced from ref. 50 with permission from Copyright 2010 American Chemical Society. (C) Laser scribing of high performance and flexible graphene-based supercapacitors. Reproduced from ref. 51 with permission from Copyright 2012 The American Association for the Advancement of Science. (D) Superior and tunable photomechanical actuator. Reproduced from ref. 53 with permission from Copyright 2015 Wiley-VCH. (E) 2D nanofluidic generators. Reproduced from ref. 54 with permission from Copyright 2013 Wiley-VCH. (F) Ultrafast viscous water filter. Reproduced from ref. 55 with permission from Copyright 2013 Nature Publishing Group.